Article
Vol. 27, No. 2, p. 139–160, April 2023
https://doi.org/10.1007/s12303-022-0030-1
pISSN 1226-4806 eISSN 1598-7477
Geosciences Journal GJ

Petrogenesis of lavas from Mokolo-Kosséhone region, northernmost segment of the Cameroon Volcanic Line: constraints from major/trace elements and Sr-Nd-Pb isotopic data

Rikangsou Tchouhla[1], Merlin Gountié Dedzo[2*], Boris Chako-Tchamabé[3], Gervais Onana[1], Djamilatou Diddi Hamadjoda[1], Pierre Christel Biakan à Nyotok[1], Klamadji Moussa Ngarena[4], Asobo Nkengmatia Elvis Asaah[5,6], and Pierre Kamgang[7]

[1]Department of Earth Sciences, Faculty of Sciences, University of Maroua, PO Box 814, Maroua, Cameroon
[2]Department of Life and Earth Sciences, High Teachers' Training College, University of Maroua, PO Box 55, Maroua, Cameroon
[3]Instituto de Investigaciones en Ciencias de la Tierra, Universidad Michoacana de San Nicolás de Hidalgo, Santiago Tapia 403, 58000, Morelia, Michoacán, Mexico
[4]Département des Sciences de la Vie et de la Terre, Faculté des Sciences Techniques et de la Technologie, Université de Pala, Pala, Tchad
[5]Department of Mines, Ministry of Mines, Industry and Technological Development, PO Box 70, Yaoundé, Cameroon
[6]Department of Earth and Planetary Sciences, Tokyo Institute of Technology, 2-12-1, Ookayama, Meguro-Ku, Tokyo 152-8551, Japan
[7]Department of Earth Sciences, University of Yaoundé I, B.P. 812 Yaoundé, Cameroon

ABSTRACT: This study presents major and trace elements, and Sr-Nd-Pb isotope data of the Mokolo-Kosséhone volcanic rock (basanite, trachybasalt, trachyte, and rhyolite) from the northernmost segment of the Cameroon Volcanic Line (CVL). The basanite sample exhibits primitive character (MgO: 12–14 wt%; Mg#: 69–72; Ni: 327–427 ppm; Cr: 524–599 ppm; Co: 57–60 ppm). Trace element and isotopic signatures of the mafic lavas are similar to those of OIB. The trends observed in the major oxides and compatible trace elements against SiO_2 from basanite to rhyolite are attributed to the fractionation of different mineral phases such as Fe-Ti oxides, olivine, clinopyroxene, feldspar, and quartz. The enrichment in LREEs and depletion in HREEs associated with $(La/Yb)_N > 5$ (12.39–32.65), $(Tb/Yb)_N > 1.7$ (1.71–2.89), and $Dy/Yb > 2$ (2.16–3.63), suggest the presence of a garnet phase in a mantle source. The lavas were produced at varying depths by low degrees of partial melting (< 4%) of a source containing less than 5% of garnet peridotite. The $^{206}Pb/^{204}Pb$ values of basanite (19.69630–19.79122) are similar to those of FOZO ($^{206}Pb/^{204}Pb > 19.5$). The trachybasalt samples with $^{206}Pb/^{204}Pb$ values of 19.25 and 19.37 suggest the probable enrichment of magma with a high-μ (HIMU) signature ($^{206}Pb/^{204}Pb < 19.5$) by a crustal component. Trace elements and isotopic compositions ($^{87}Sr/^{86}Sr$: 0.70308–0.70378, $^{143}Nd/^{144}Nd$: 0.51287–0.51296, $^{206}Pb/^{204}Pb$: 19.24652–19.79122) of the Mokolo-Kosséhone lavas are consistent with a mixture of different source material from the sub-continental lithospheric mantle (SCLM) and the asthenosphere with minor crustal contamination. The composition of the source is analogous to those described in the northern portion of the CVL and other volcanic massifs along the CVL.

Key words: Cameroon Volcanic Line, Mokolo-Kosséhone, focal zone, high-μ mantle, sub-continental lithospheric mantle

Manuscript received July 19, 2022; Manuscript accepted October 13, 2022

1. INTRODUCTION

The administrative Far North Region of Cameroon is situated in the northernmost section of the Cameroon volcanic line (CVL). It is characterized by various volcanic geoforms, which testify to the intensive volcanic activity that occurred in this region. Cameroon volcanism has been associated with a system of N30°E and N70°E fractures (Fig. 1a, b) localized in a corridor stretching about 100 km wide and approximately 1600 km in

Editorial responsibility: Ian Smith

***Corresponding author:**
Merlin Gountié Dedzo
Department of Life and Earth Sciences, High Teachers' Training College, University of Maroua, PO Box 55, Maroua, Cameroon
Tel: +237-675088586, E-mail: merlin.gountie@gmail.com

length from the Gulf of Guinea to Chad. Along the line, the main volcanic edifices include the islands of Bioko, Sao Tome, Principe, and Pagalu located in the Guinea Gulf. Mts. Bambouto, Manengouba, Oku, and Mandara found within the Cameroonian land. These mountains are often separated by monogenetic volcanic fields in which several plutonic or anorogenetic complexes and small volume volcanoes such as maars, scoria cones, and short lava flows are exhibited.

Known as the northernmost end of the continental part of the CVL where the study area is situated, the Mts. Mandara are located along the Cameroon-Nigeria border and run about 450 km from Adamawa Region to the Far North Region of Cameroon. This northern part of the CVL remains one of the areas where geochemical studies are limited. Nevertheless, some earlier petrological work carried out in this sector of the CVL (e.g., Kapsiki Plateau and its vicinity, Ngounouno et al., 2000; Tamen

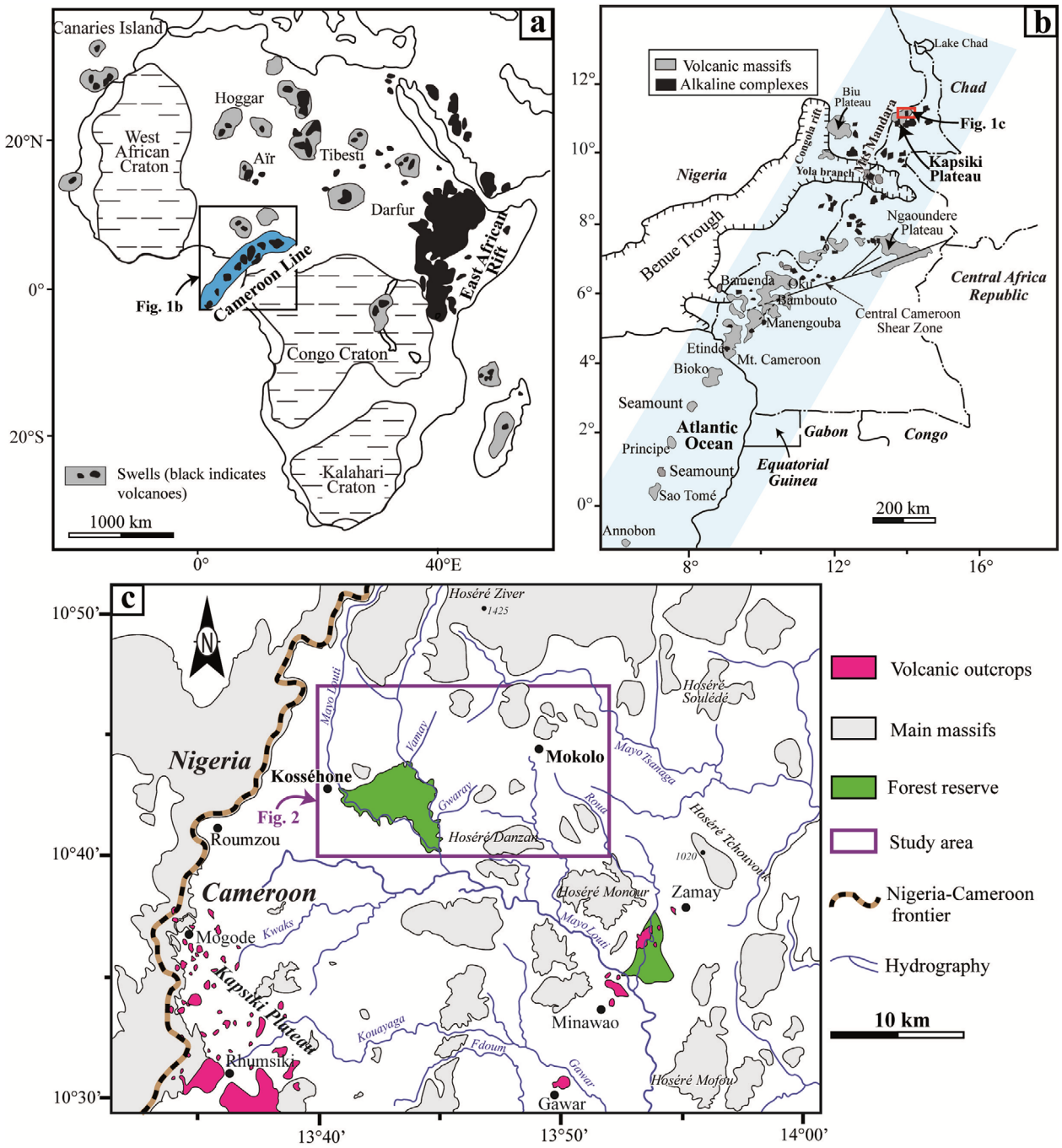

Fig. 1. (a) Location map of the Cameroon Volcanic Line (CVL). The principal geological features of Africa are also shown. (b) Main alkaline complexes and volcanic massifs of the CVL. (c) Simplified geological map of the Kapsiki Plateau and vicinity; volcanic outcrops are from Ngounouno et al. (2000), Tamen et al. (2015) and Gountié Dedzo et al. (2019).

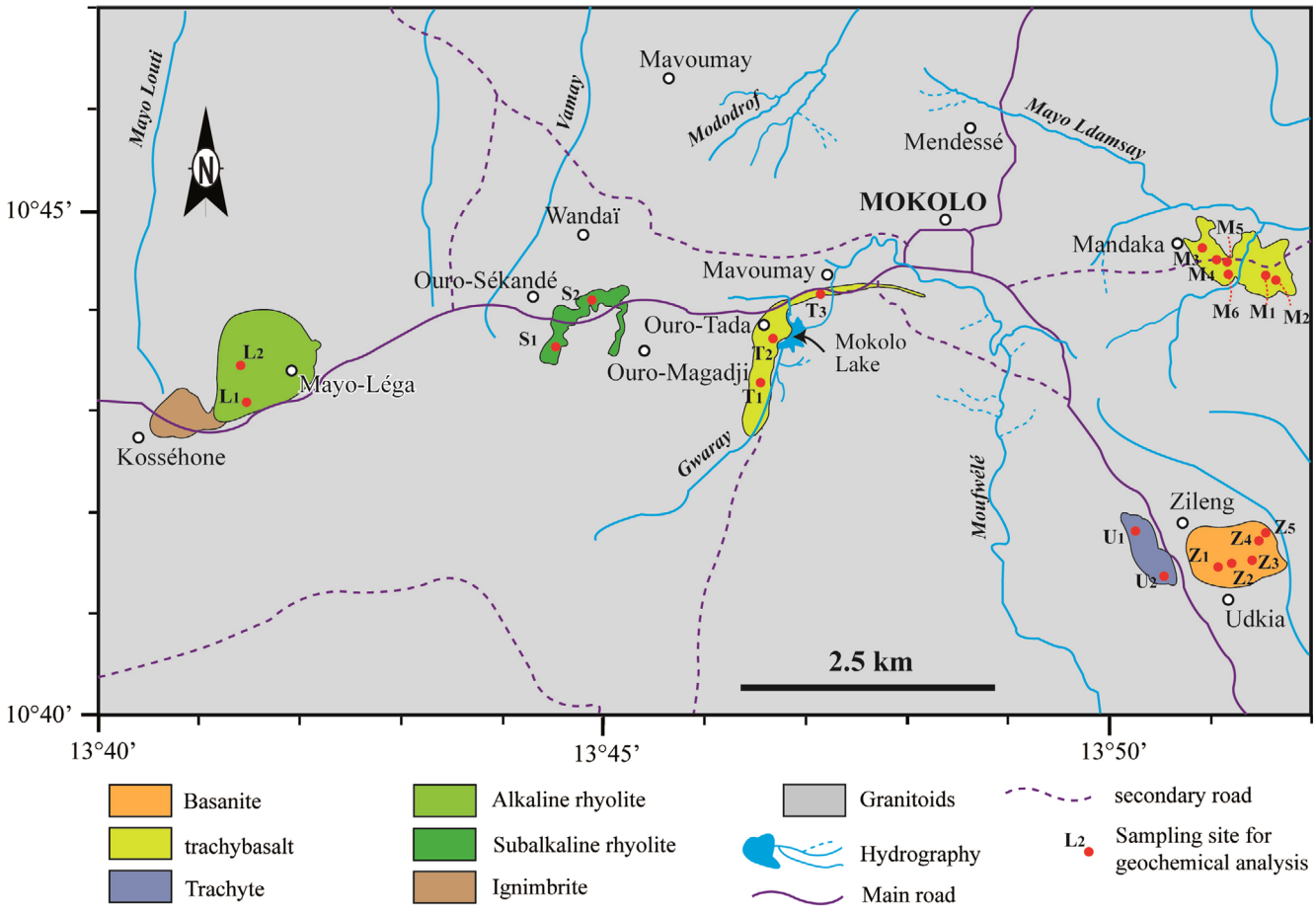

Fig. 2. Geologic map of the study area. Sampling sites for geochemical analysis are also indicated.

et al., 2015; Gountié Dedzo et al., 2019; Biu and Jos Plateau, Rankenburg et al., 2005) had deepened the understanding of the genesis of volcanic formations and the mechanisms of this megastructure.

In this study, major and trace elements and Sr-Nd-Pb isotope systematics of lavas from the Mokolo-Kosséhone region, situated between 13°40′E and 13°52′E and 10°40′N and 10°47′N (Fig. 1c), are used to constrain the mantle source composition of volcanic rocks (Fig. 2) present in this area and compare them to nearby volcanic centers.

2. GEOLOGICAL BACKGROUND

Like the Rift Valleys system and Benue trough, the Cameroon Volcanic Line (CVL) represent a mega tectono-magmatic structure in Africa (Déruelle et al., 2007). It is a chain of Cenozoic volcanoes extending over a distance of 1600 km from the Atlantic Ocean (Gulf of Guinea) to Africa continent. This succession of unimodal (only some volcanoes, e.g., Mts. Cameroon and Etinde) and bimodal (most volcanoes, e.g., Kapsiki and Ngaoundere Plateaux, Mts. Oku, Bamenda, Bambouto and Manengouba) volcanoes is made up of volcanic products comprising primitive mafic (basanites, basalts) and more differentiated (trachytes, phonolites, rhyolites and ignimbrites) rocks dated from 51.8 Ma (Bamoun Plateau) to the present (Mt. Cameroon) (Sato et al., 1990; Marzoli et al., 2000; Suh et al., 2003; Fosso et al., 2005; Moundi et al., 2007; Kamgang et al., 2013; Njome and de Wit, 2014; Asaah et al., 2015a, 2020, 2021; Gountié Dedzo et al., 2019, 2020, 2022). The northern segment of the CVL is made up by important volcanic plateaus including the Ngaoundéré, Kapsiki, Biu plateaus, and the Mts. Mandara (Fig. 1b).

The age of volcanic activities nearby Ngaoundéré locality are Oligocene (Itiga et al., 2013), to Mio-Pliocene and Pleistocene (Letterman, 1984). Hydro-magmatic explosive activity associated to approximately sixty eruptive centers including maars and plugs have been described in the Ngaoundéré region (Nkouandou et al., 2008). The Ngaoundéré Plateau is characterized by the diversity of their volcanic centers and their products (basalt, trachyte, phonolite and volcanic breccias) which suggests multiple eruptive styles (Nono et al., 1994; Marzoli et al., 1999, 2000; Tiabou et al., 2019).

The volcanic activities of the Kapsiki Plateau and its vicinity

https://doi.org/10.1007/s12303-022-0030-1

are characterized by setting up of alkaline lavas with a classically bimodal series comprising felsic (rhyolites, phonolites and trachytes) and mafic (hawaiite, basanite and basalts) lavas (Ngounouno et al., 2000; Tamen et al., 2015; Gountié Dedzo et al., 2019).

The Biu Plateau was built in three phases during two episodes of volcanism: (i) an initial fissure type eruption; (ii) building up of tephra ring volcanic centres and formation of thick lava piles (basanite, basalt and trachybasalt up to 250 m) in the southern portion of the plateau ages from 5.35 to 0.84 Ma (Grant et al., 1972; Fitton and Dunlop, 1985; Rankenburg et al., 2005); (iii) Renewal of igneous activity with the building up of over 80 NNW-SSE-aligned cinder cones with ages estimation of 0.50 to 0.25 Ma and comparable chemistry to the previous (5.35 to 0.84 Ma) basalts (Barfod et al., 1999; Salzmann, 2000; Rankenburg et al., 2005).

The Mts. Mandara which culminate at 1412 m, are formed by a series of plateaus with flats continuously at 650 m, 750 m and 1000 m in the direction of the Kapsiki Plateau. The mafic lavas of this massif comprise basanites, basalts, hawaiites and mugearites with mantle xenolith enclaves. Felsic rocks are also found including benmoreites, trachytes, phonolites and rhyolites (Nono et al., 1994; Marzoli et al., 1999, 2000; Déruelle et al., 2000; Ngounouno et al., 2000; Rankenburg et al., 2005; Tamen et al., 2015). New outcrops of volcanic rocks identified during our field investigations will be studied to update the petrological data of Mts Mandara.

3. ANALYTICAL TECHNIQUES

Major and trace element and isotope data were obtained for 20 volcanic rocks from the Mokolo-Kosséhone study area (7 from Udkia, 6 from Mandaka, 3 from Ouro-Tada, 2 from Ouro-Sékandé and 2 from Mayo-Léga, Fig. 2). Sample preparation, digestion, and analytical procedures were done following Asaah et al. (2020, 2021). Major (with some minor elements, including Cr, Co, Ni, V and Sc) were analyzed by X-ray fluorescence (XRF) spectrometry, using a Rigaku RIX 2100 at the Graduate School of Science, Osaka University in Japan. Approximately 50 mg of rock powders were digested using HF, HNO_3 and $HClO_4$ following the method described by Yokoyama et al. (1999), and utilized for the determination of lithophile trace elements (Rb, Sr, Y, Cs, Ba, REEs, Pb, Th and U). The abundances of these elements were determined with inductively coupled plasma mass spectrometry (ICP-MS; X-series II, Thermo-Fisher Scientific) at the Tokyo Institute of Technology, Japan, by the calibration curve method with double internal standards (In + Tl) using a reference rock material JB-3 (basalt; Geological Survey of Japan) as the standard (Yokoyama et al., 2017). High field strength elements (Zr, Nb, Hf and Ta) were separately analysed following the method described in Makishima et al. (1999). Typical analytical precision (2σ) were 5% for Y and Ta, 4% for Nb and Pb and < 3% for the rest of the trace elements.

Isotope analyses for Pb, Nd and Sr were also performed using thermal ionisation mass spectrometry (TIMS), Triton plus (Thermo-Fisher Scientific) at the Tokyo Institute of Technology. The ratios of $^{143}Nd/^{144}Nd$ and $^{87}Sr/^{86}Sr$ were corrected for internal mass fractionation using $^{146}Nd/^{144}Nd = 0.7219$ and $^{86}Sr/^{88}Sr = 0.1194$, respectively. Repeated analyses of standard materials NIST 987 (measured value: $^{87}Sr/^{86}Sr = 0.710264 \pm 3$) and JNdi-1 (measured value: $^{143}Nd/^{144}Nd = 0.512108 \pm 1$) was used to correct the results for Sr and Nd, respectively. Measurements of these standards were carried out during the same analytical period and were finally normalised using the recommended values of $^{87}Sr/^{86}Sr = 0.71025$ (accepted NIST 987) and $^{143}Nd/^{144}Nd = 0.512115$ (Tanaka et al., 2000). Typical analytical reproducibility (2σ) was 0.005% for Sr and Nd. Lead isotope ratios were precisely measured by the standard "double spike method" using the ^{204}Pb-^{207}Pb spikes as described in Hamelin et al. (1985), Kuritani and Nakamura (2003) and Rudge et al. (2009). Typical analytical precision (2σ) for $^{206}Pb/^{204}Pb$, $^{207}Pb/^{204}Pb$ and $^{208}Pb/^{204}Pb$ were 0.01%.

4. RESULTS

4.1. Nomenclature, Field Occurrence and Petrography

The Total Alkali Silica (TAS) classification of Le Bas et al. (1986) which was chosen for the nomenclature of the studied rocks is based on the variation of the sum of the alkali as a function of the SiO_2 content (Fig. 3a). The alkaline-subalkaline dividing line of Irvine and Baragar (1971) is also associated with this diagram. Like most of the rocks in the northern part of CVL, the samples range from mafic rocks (basanite, trachybasalt) to felsic rocks (trachyte, alkaline and subalkaline rhyolites) (Fig. 3a). The normative olivines in basanite varies between 23.17% to 25.6%. The mafic lavas are silica-undersaturated with normative nepheline fluctuating from 1.08% to 11.98%. Except for subalkaline rhyolites, all the samples show alkaline affinity according to this diagram. In the Na_2O versus K_2O diagram (Middlemost, 1975) (Fig. 3b), the basanites fall within the Na-series field (Na_2O/K_2O = 2.21–2.59); while trachybasalt, trachyte, and rhyolite plot in the K-series field (Na_2O/K_2O = 1.49–0.67). Majority of the rocks are characterized by high alkalinity index ($(Na_2O + K_2O) - (0.37 \times SiO_2 - 14.43)$) which vary from 2.05 to 2.80. Using the classification of Le Maitre (2002), the mafic lavas are ultrapotassic whereas the felsic ones are high-K (rhyolite) and ultapotassic (trachyte) (Fig. 3c).

Basanites and trachybasalts outcrop as blocks and lava flows in Udkia, Mandaka and Ouro-Tada localities (Fig. 4a–c). They exhibit microlitic porphyritic texture (phenocrysts ≥ 10 vol%)

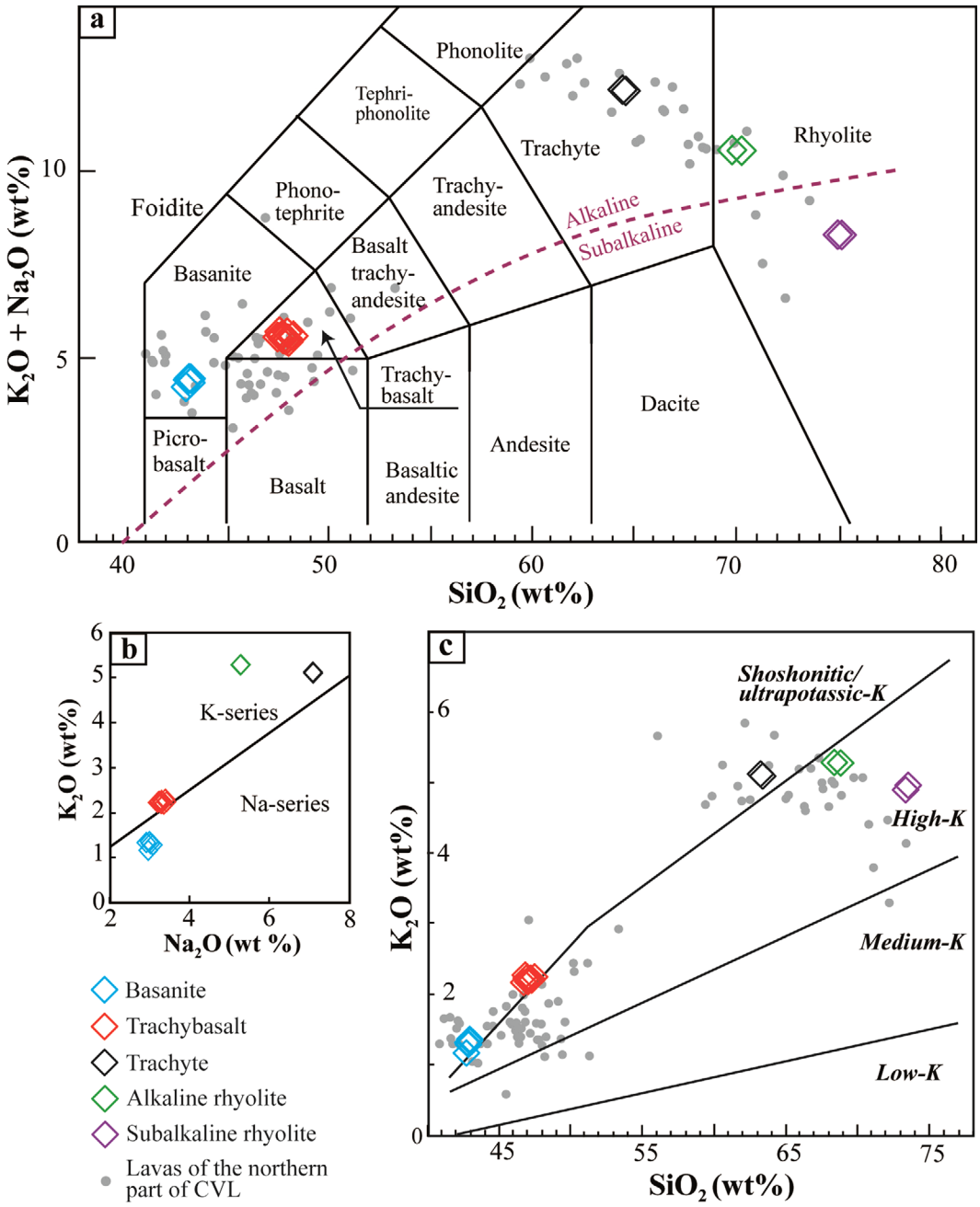

Fig. 3. (a) TAS (Total alkali versus silica) classification diagram (after Le Bas et al., 1986); the alkaline-subalkaline dividing line is from Irvine and Baragar (1971). (b) K_2O versus Na_2O diagram of the alkaline series (Middlemost, 1975). (c) K_2O versus SiO_2 (Le Maitre, 2002). Data sources of the northern part of the CVL are also shown (Marzoli et al., 1999, 2000; Ngounouno et al., 2000; Rankenburg et al., 2005; Gountié Dedzo et al., 2019).

under microscope. The phenocryst phases are principally olivine, clinopyroxene, amphibole and oxides (Fig. 5a–c). Peridotite xenoliths are present in some basanites and trachybasalts (Figs. 4a, c, and 5c) as observed in the field and in the thin sections. The proportion of olivine is more abundant in basanite (~30 vol%) compared to trachybasalt (~15 vol%). Olivine sections often show marks for iddingsitisation. The groundmass of trachybasalt and basanite comprises plagioclases microlites associated with microcrysts of olivine, clinopyroxene and oxides.

Trachytes outcrop as a dome with a splitting in blocks (Fig. 4d) in Udkia and show microlitic aphyric texture (phenocrysts ≤ 3 vol%). The rare phenocrysts are mainly sanidine and plagioclase (Fig. 5d). Plagioclases (about 75 vol%) are the most abundant phase present in the groundmass while other microcrysts such as clinopyroxene, amphibole, biotite and opaque minerals are also noted.

https://doi.org/10.1007/s12303-022-0030-1

Fig. 4. Field photos of the studied lavas. (a) basanite of Udkia, the length of the pen cap is 5.5 cm, (b) trachybasalt of Ouro-Tada, (c) trachybasalt of Mandaka, the length of the marker in 14 cm, (d) Trachyte of Udkia, (e) Alkaline rhyolite of Sékandé, the length of the hammer is 33 cm, (f) subalkaline rhyolite of Kosséhone.

Alkaline rhyolite outcrops as an annular dome presenting a chaotic surface (Fig. 4e) in Sékandé and exhibit microlitic porphyritic texture (phenocrysts ≥ 5 vol%; these phenocrysts are mostly sanidines). Alkali feldspar (75 vol%) and plagioclase (15 vol%) are the main mineral phase (Fig. 5e). Other crystals with lesser proportions such as clinopyroxene, biotite, quartz and oxides are found in groundmass.

Subalkaline rhyolite (Fig. 4f) outcrops as a asymmetrical dome in Kosséhone and displays microlitic aphyric texture (phenocrysts ≤ 3 vol% and represented by sanidine and quartz).

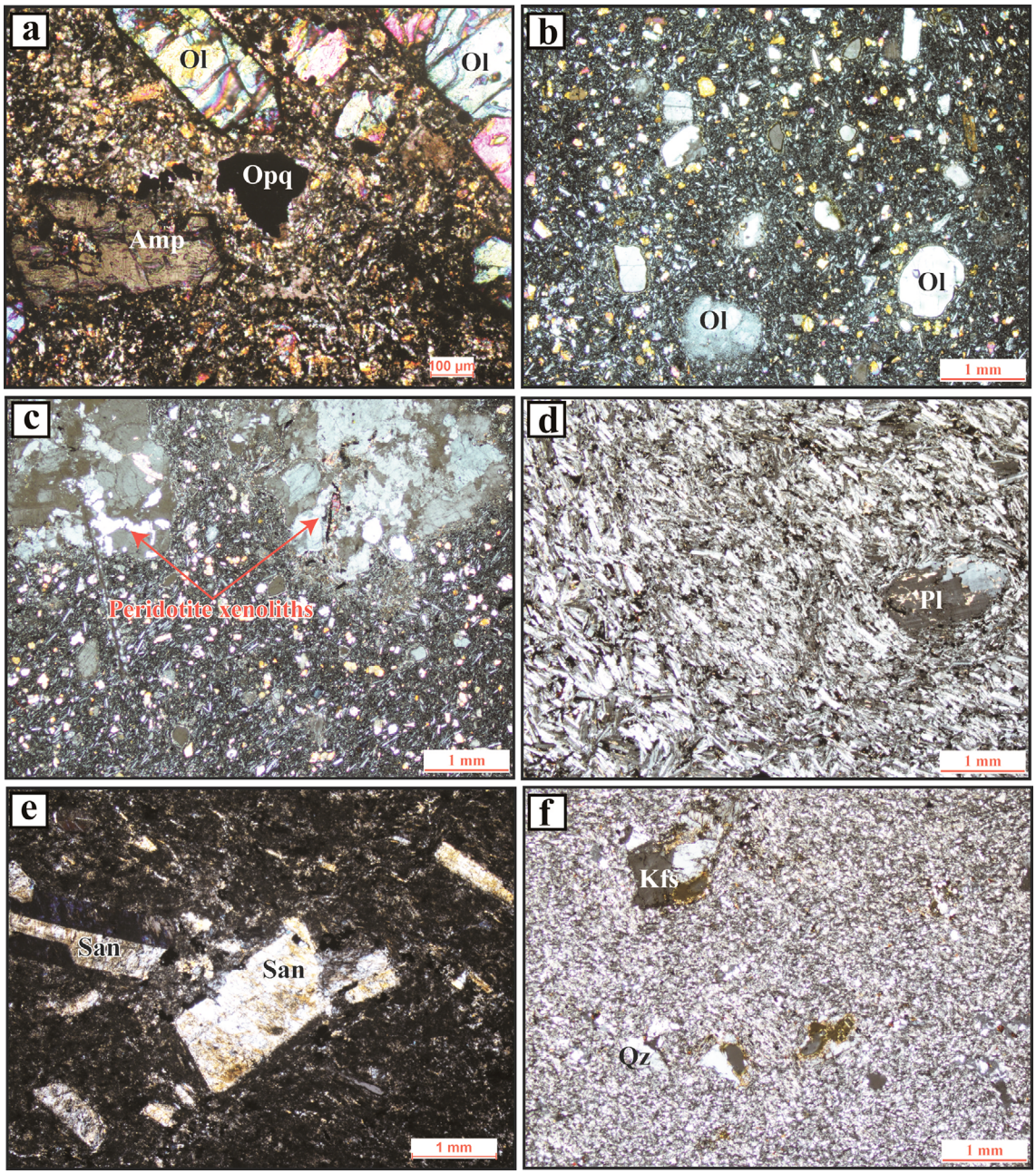

Fig. 5. Photomicrographs of rock samples from study area. (a) basanite of Udkia, (b and c) trachybasalt of Mandaka, (d) trachyte of Udkia, (e) alkaline rhyolite of Kosséhone, (f) subalkaline rhyolite of Udkia. Ol: olivine; Opq: opaque mineral; Amp: amphibole; Pl: plagioclase; San: sanidine; Kfs: alkali feldspar.

Alkali feldspar (40 vol%), plagioclase (10 vol%) and quartz (20 vol%) are the most abundant crystal phase (Fig. 5f). Microcrysts of the same minerals are also present in the groundmass.

4.2. Geochemistry

Major and trace elements data for representative samples of the Mokolo-Kosséhone lavas are presented in Table 1.

4.2.1. Major oxides

The concentrations of major elements of the studied lavas are in the same range as that of the northern part of the CVL as seen in Figures 3 and 6. The mafic lavas (SiO_2: 42.93–48.23 wt%) of the study area have a Mg number (Mg#) varying from 69.40 to 72.00 for the basanites and from 49.80 to 60.30 for the trachybasalts. The Mg# (> 68) and MgO (> 10 wt%) of the basanite are within the compositional range of primary magmas. The felsic lavas are characterized by high SiO_2 (64.44–75.24 wt%) and low MgO

https://doi.org/10.1007/s12303-022-0030-1

Table 1. Major (wt%) and trace (ppm) element data for the Mokolo-Kosséhone lavas

Locality	Udkia					Mandaka					
Rock type	Basanite					Trachybasalt					
Sample ID	Z1	Z2	Z3	Z4	Z5	M1	M2	M3	M4	M5	M6
Longitude (E)	13°51′06.3″	13°51′15.6″	13°51′23.5″	13°51′29.8″	13°51′32.3″	13°51′27.2″	13°51′31.4″	13°50′58.1″	13°51′01.1″	13°51′12.5″	13°51′13.7″
Latitude (N)	10°41′28.8″	10°41′29.7″	10°41′32.1″	10°41′48.2″	10°41′51.4″	10°44′20.9″	10°44′16.5″	10°44′42.6″	10°44′38.9″	10°44′29.1″	10°44′20.2″
ICP-AES major element data (wt%)											
SiO_2	42.93	43.08	43.03	43.15	43.17	47.62	47.92	47.73	47.84	48.23	47.55
TiO_2	2.38	2.36	2.38	2.45	2.41	2.93	2.91	2.94	2.93	2.89	2.95
Al_2O_3	11.75	11.75	11.76	12.27	12.12	14.62	14.67	14.67	14.60	14.70	14.68
Fe_2O_3t	12.18	12.06	12.06	12.21	12.14	10.75	10.70	10.78	10.81	10.62	10.78
MnO	0.18	0.18	0.18	0.18	0.19	0.16	0.16	0.16	0.16	0.15	0.16
MgO	13.57	13.80	13.69	12.34	12.73	7.14	7.05	7.14	7.22	6.98	6.97
CaO	10.34	10.14	10.18	10.48	10.21	8.41	8.34	8.50	8.47	8.29	8.43
Na_2O	2.99	3.10	3.04	2.94	3.02	3.33	3.44	3.31	3.25	3.32	3.42
K_2O	1.16	1.28	1.31	1.33	1.35	2.19	2.18	2.14	2.18	2.21	2.23
P_2O_5	0.56	0.55	0.56	0.58	0.57	0.63	0.63	0.63	0.63	0.62	0.63
Total	98.04	98.32	98.19	97.93	97.91	97.78	97.99	97.99	98.08	98.02	97.80
$Na_2O + K_2O$	4.15	4.38	4.34	4.27	4.37	5.52	5.62	5.45	5.43	5.53	5.65
Mg#	71.40	72.00	71.80	69.40	70.20	59.90	59.70	49.80	60.00	59.60	59.30
ICP-MS trace elements data (ppm)											
Sc	27.49	27.51	28.46	28.17	27.57	23.01	22.60	22.95	22.13	21.60	21.80
V	214.62	212.84	212.26	220.06	216.65	191.19	189.22	190.13	191.48	186.81	196.08
Cr	549.73	599.10	593.34	546.11	524.11	107.65	109.44	110.34	111.55	101.66	111.41
Co	59.18	59.47	59.66	56.93	57.53	41.18	40.68	39.92	42.13	40.70	40.82
Ni	410.82	427.39	421.92	327.45	351.74	91.92	89.54	89.91	91.72	84.73	91.29
Cu	63.94	54.60	64.89	56.62	64.96	32.46	31.69	32.70	31.96	28.65	31.31
Zn	97.03	95.16	96.31	98.69	99.69	90.88	90.38	92.27	91.44	90.43	90.20
Ga	16.82	17.97	17.55	17.69	18.57	19.27	19.91	19.43	19.03	20.01	19.26
Rb	30.50	34.50	36.05	32.51	33.66	55.03	60.86	59.57	63.05	61.92	63.97
Sr	944.64	846.01	1324.46	1378.59	861.66	1116.33	1061.43	1164.42	1443.33	1149.73	1158.67
Y	24.09	23.34	24.43	24.66	24.75	22.92	25.07	25.19	27.00	25.45	25.28
Cs	0.28	0.43	0.46	0.35	0.48	0.57	0.57	0.47	0.74	0.93	0.96
Ba	451.75	451.98	482.09	499.24	475.65	631.85	578.48	608.78	557.90	585.79	583.00
La	39.59	39.38	41.47	42.33	40.86	58.74	53.94	54.56	52.94	53.54	53.90
Ce	103.80	103.17	129.43	132.41	106.69	178.93	165.07	167.54	142.18	163.98	164.78
Pr	9.94	9.58	9.81	10.02	9.92	14.25	13.05	13.24	12.77	12.96	13.01
Nd	37.57	37.15	39.96	40.87	38.34	57.44	51.76	52.13	49.55	51.54	51.92
Sm	7.63	7.52	8.10	8.32	7.80	11.16	9.95	10.00	9.47	10.05	10.09
Eu	2.50	2.44	2.58	2.65	2.53	3.42	2.97	2.97	2.91	2.95	3.04
Gd	6.75	6.68	7.06	7.24	6.90	9.42	8.10	8.09	8.00	8.19	8.30
Tb	0.96	0.93	0.97	1.00	0.98	1.28	1.10	1.09	1.08	1.10	1.11
Dy	5.02	4.91	5.22	5.41	5.16	6.91	5.85	5.75	5.60	5.85	5.92
Ho	0.91	0.88	0.92	0.96	0.93	1.21	1.02	1.00	1.00	1.01	1.02
Er	2.24	2.17	2.30	2.41	2.31	3.06	2.55	2.50	2.46	2.55	2.59
Tm	0.29	0.28	0.29	0.31	0.30	0.40	0.33	0.32	0.32	0.33	0.33
Yb	1.72	1.66	1.71	1.82	1.79	2.35	1.93	1.88	1.89	1.92	1.94
Lu	0.24	0.23	0.24	0.26	0.25	0.33	0.27	0.27	0.26	0.27	0.27
Pb	2.44	2.61	2.35	2.48	2.63	7.45	5.59	5.19	5.35	5.43	5.42
Th	4.94	4.63	4.47	4.60	5.17	12.61	9.09	8.50	8.81	7.85	8.52
U	1.30	1.29	1.18	1.21	1.36	3.43	2.29	2.13	2.08	1.89	2.10
Zr	162.02	184.06	193.93	199.04	187.07	319.68	320.70	317.26	310.38	314.78	323.78
Hf	3.83	4.37	4.42	4.48	4.46	7.05	7.12	7.07	7.06	6.97	7.13
Nb	59.57	59.68	119.26	103.37	62.23	39.50	39.23	39.52	69.08	39.86	39.80
Ta	1.34	1.53	1.53	1.54	1.53	2.42	2.44	2.44	2.37	2.40	2.45
Eu/Eu*	1.06	1.05	1.04	1.04	1.06	1.02	1.01	1.01	1.02	0.99	1.01
Nb/Nb*	1.44	1.50	2.97	2.51	1.45	0.49	0.60	0.62	1.08	0.66	0.63
$^{143}Nd/^{144}Nd$	0.51295	0.51296			0.51295				0.51287		
$^{87}Sr^{86}Sr$	0.70354	0.70308			0.70313				0.70378		
$^{206}Pb/^{204}Pb$	19.73341	19.79122			19.69630				19.24652		
$^{207}Pb/^{204}Pb$	15.70973	15.71173			15.70965				15.71259		
$^{208}Pb/^{204}Pb$	39.47033	39.52155			39.44921				39.86865		

Mg# = 100 × (MgO/40.31)/((MgO/40.31 + Fe_2O_3 × 0.8998/(71.85/(1 − 0.15))), assuming FeOt = Fe_2O_3 × 0.8998Fe_2O_3.

Table 1. (continued)

Locality	Ouro-Tada			Udkia		Mayo-Léga		Ouro-Sékandé	
Rock type	Trachybasalt			Trachyte		Alkaline rhyolite		Subalkaline rhyolite	
Sample ID	T1	T2	T3	U1	U2	L1	L2	S1	S2
Longitude (E)	13°51′24″	13°51′23.5″	13°46′46.4″	13°50′21.3″	13°50′40.6″	13°41′51.7″	13°41′57.4″	13°41′31″	13°41′28.2″
Latitude (N)	10°44′28.3″	10°44′30.8″	10°44′02.4″	10°41′54.2″	10°41′23.4″	10°43′09.6″	10°43′20.1″	10°43′03″	10°43′22.3″
ICP-AES major element data (wt%)									
SiO_2	47.44	47.94	48.00	64.60	64.44	69.84	70.31	75.06	75.24
TiO_2	2.97	2.93	2.94	0.20	0.20	0.28	0.28	0.09	0.09
Al_2O_3	14.63	14.64	14.62	15.48	15.50	14.47	14.61	13.40	13.40
Fe_2O_3t	10.87	10.74	10.77	4.81	4.86	2.93	2.90	1.59	1.56
MnO	0.16	0.16	0.16	0.14	0.15	0.03	0.03	0.02	0.02
MgO	7.26	7.17	7.29	0.06	0.06	0.16	0.16	0.14	0.13
CaO	8.44	8.36	8.29	0.76	0.78	0.13	0.13	0.34	0.21
Na_2O	3.38	3.27	3.22	7.10	7.10	5.30	5.28	3.39	3.32
K_2O	2.13	2.19	2.16	5.09	5.12	5.28	5.27	4.89	4.96
P_2O_5	0.64	0.63	0.64	0.03	0.03	0.01	0.01	0.01	0.01
Total	97.90	98.03	98.07	98.26	98.22	98.43	98.98	98.91	98.94
$Na_2O + K_2O$	5.50	5.46	5.38	12.19	12.21	10.58	10.56	8.28	8.27
Mg#	60.00	60.00	60.30						
ICP-MS trace elements data (ppm)									
Sc	21.53	23.04	21.52	0.60	0.37	0.34	b.d.l.	0.07	b.d.l.
V	193.54	192.03	187.27	3.40	3.83	6.00	3.04	3.59	3.70
Cr	108.68	103.93	107.18	b.d.l.	b.d.l.	b.d.l.	b.d.l.	2.15	5.86
Co	42.32	42.26	41.86	1.60	2.97	2.50	2.70	2.32	1.71
Ni	89.86	88.91	90.33	0.87	1.35	2.59	2.91	5.17	4.63
Cu	32.62	27.94	33.47	2.23	3.11	0.20	-0.92	3.43	2.07
Zn	91.02	91.62	91.71	236.88	231.13	143.00	142.45	106.67	106.04
Ga	19.22	20.00	19.43	42.92	41.08	37.30	36.83	34.39	34.80
Rb	60.96	63.05	60.01	157.28	155.86	164.03	168.52	347.11	351.66
Sr	1356.68	1591.63	1513.11						
Y	27.87	24.58	24.13	129.12	120.38	140.97	125.85	126.23	93.62
Cs	0.56	0.84	1.09	0.93	0.96	0.27	0.27	1.86	1.81
Ba	555.18	613.85	628.90	28.70	33.90	32.55	17.67	43.58	45.65
La	52.48	84.63	89.07	282.71	278.27	139.75	162.31	184.10	175.75
Ce	139.90	170.00	179.12	550.11	541.57	238.49	248.83	223.65	219.82
Pr	12.68	13.17	13.89	41.90	46.61	22.71	27.89	49.00	46.36
Nd	49.40	52.06	55.71	142.74	148.10	91.49	94.53	120.80	113.33
Sm	9.54	9.95	10.70	25.40	25.30	20.10	19.48	26.60	25.17
Eu	2.95	2.98	3.23	1.55	1.56	1.62	1.54	0.36	0.34
Gd	8.01	8.00	8.85	19.42	18.60	19.64	17.68	18.99	17.63
Tb	1.08	1.08	1.19	3.07	3.03	3.20	2.89	3.18	2.87
Dy	5.62	5.73	6.33	17.76	17.55	18.92	16.78	17.78	16.43
Ho	1.00	0.99	1.10	3.31	3.24	3.53	3.06	2.88	2.48
Er	2.46	2.48	2.74	9.14	8.90	9.44	8.04	7.52	5.34
Tm	0.32	0.32	0.35	1.30	1.26	1.29	1.10	1.05	0.79
Yb	1.89	1.86	2.06	8.24	8.06	8.09	6.98	6.83	4.52
Lu	0.26	0.26	0.29	1.23	1.20	1.19	1.05	0.89	0.51
Pb	5.40	5.34	5.78	11.08	10.63	8.91	8.58	14.76	15.53
Th	8.97	7.57	8.19	25.39	24.75	12.60	10.75	42.96	33.22
U	2.21	1.90	2.06	4.84	4.07	2.90	2.30	7.08	6.14
Zr	320.16	312.77	300.51	1760.87	1702.87	1272.03	1163.34	223.12	95.76
Hf	7.18	6.88	7.07	35.44	34.40	27.22	25.67	11.18	5.92
Nb	70.89	38.63	40.00	223.16	208.25	77.93	125.97	189.10	264.85
Ta	2.42	2.37	2.44	11.59	11.26	8.93	8.44	3.75	2.05
Eu/Eu*	1.03	1.02	1.01	0.21	0.22	0.25	0.25	0.05	0.05
Nb/Nb*	1.44	1.50	2.97	2.51	1.45	0.49	0.60	0.62	1.08
$^{87}Sr/^{86}Sr$	0.70346								
$^{143}Nd/^{144}Nd$	0.51289								
$^{206}Pb/^{204}Pb$	19.37020								
$^{207}Pb/^{204}Pb$	15.71107								
$^{208}Pb/^{204}Pb$	39.85277								

https://doi.org/10.1007/s12303-022-0030-1

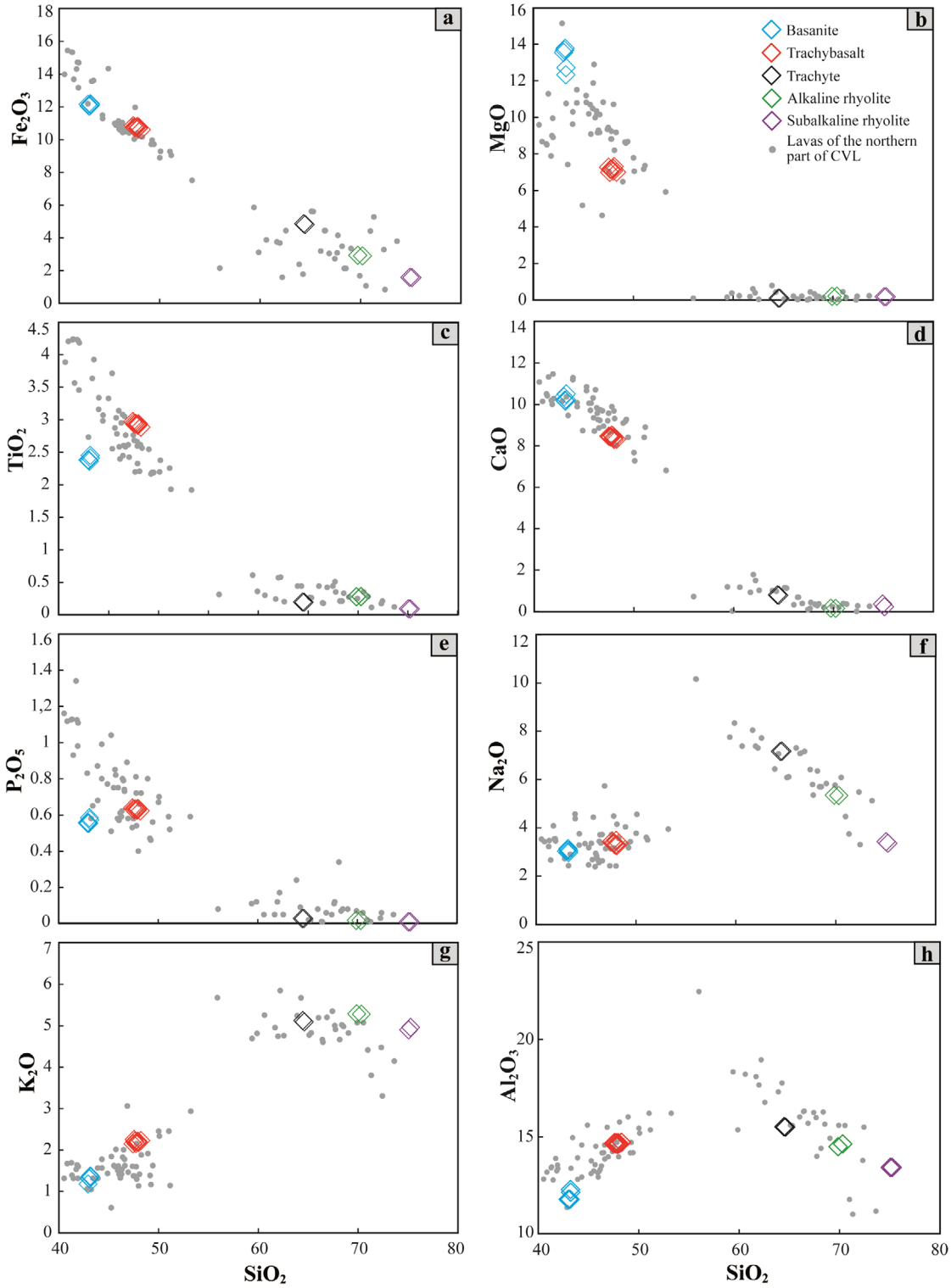

Fig. 6. (a) Major oxides variation diagrams. Data sources of the northern part of the CVL are similar to Figure 3.

(< 0.16 wt%) contents. In the Harker diagrams of major oxides versus SiO_2 (Fig. 6), Fe_2O_3, MgO, TiO_2, CaO, and P_2O_5 concentrations decrease from basanites to rhyolites with increasing SiO_2 contents (Fig. 6a–e). On the other hand, Na_2O, K_2O, and Al_2O_3 concentrations initially increase in mafic lavas and then gradually decrease in felsic ones (Fig. 6f–h).

4.2.2. Trace elements

The concentrations of Ni, Co and Cr in the mafic lavas range from 80.73 to 427.45, 39.92 to 59.66 and 101.66 to 599.10,

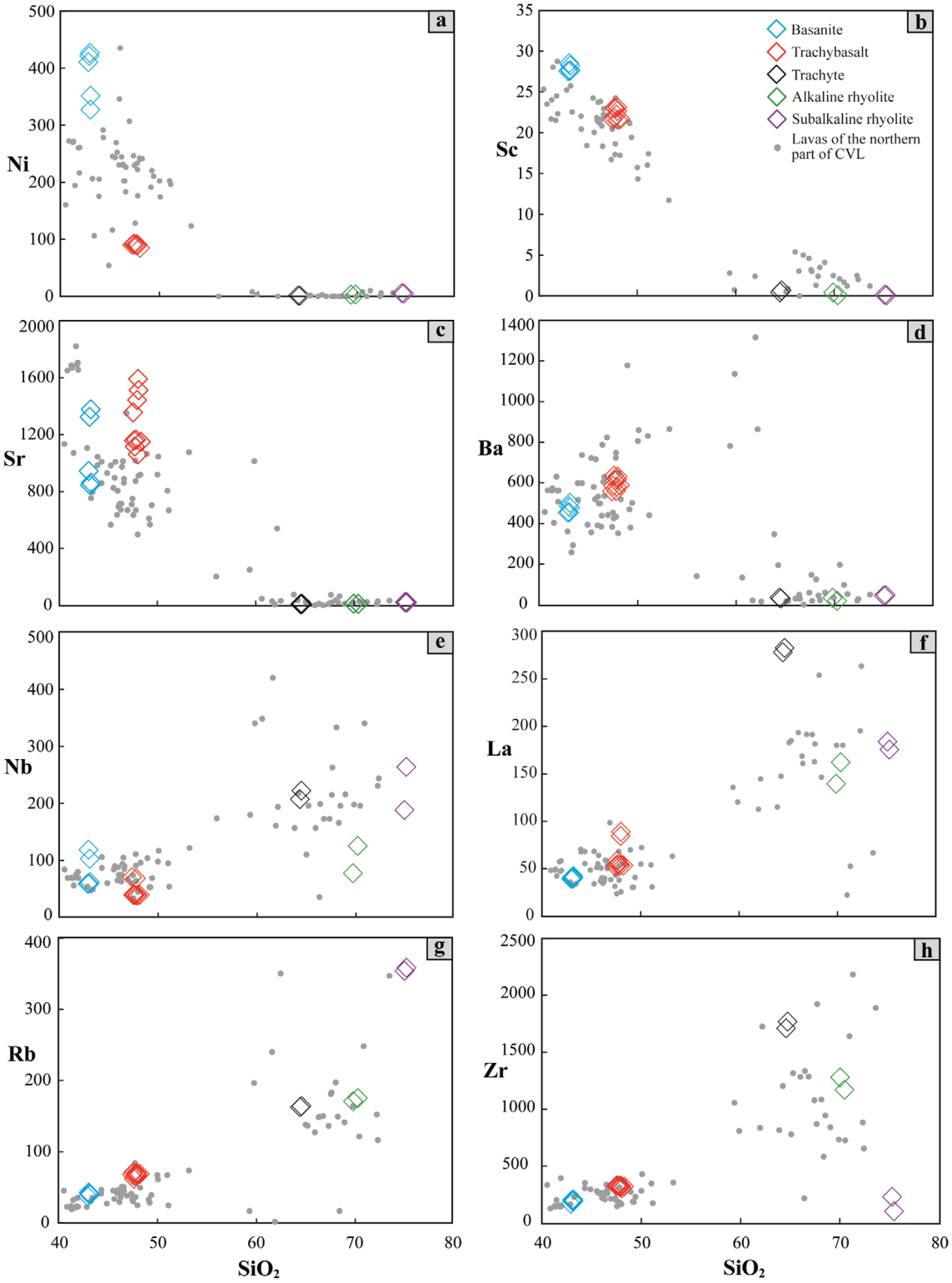

Fig. 7. (a) Trace element variation diagrams. Data sources of the northern part of the CVL are similar to Figure 3.

respectively, whereas for the felsic samples, these contents are very low (< 6 ppm). Like the major elements, the high contents of Ni (> 427 ppm), Co (> 59 ppm) and Cr (> 599 ppm) in the basanites also reflect the primitive character of this lava. Plots of SiO_2 versus selected trace elements are exhibit negative correlations with a constant decrease in Ni, Sc, Sr, and Ba contents with increasing SiO_2 concentration from mafic to felsic lavas (Fig. 7a–d), whereas positive correlations are observed with increasing

https://doi.org/10.1007/s12303-022-0030-1

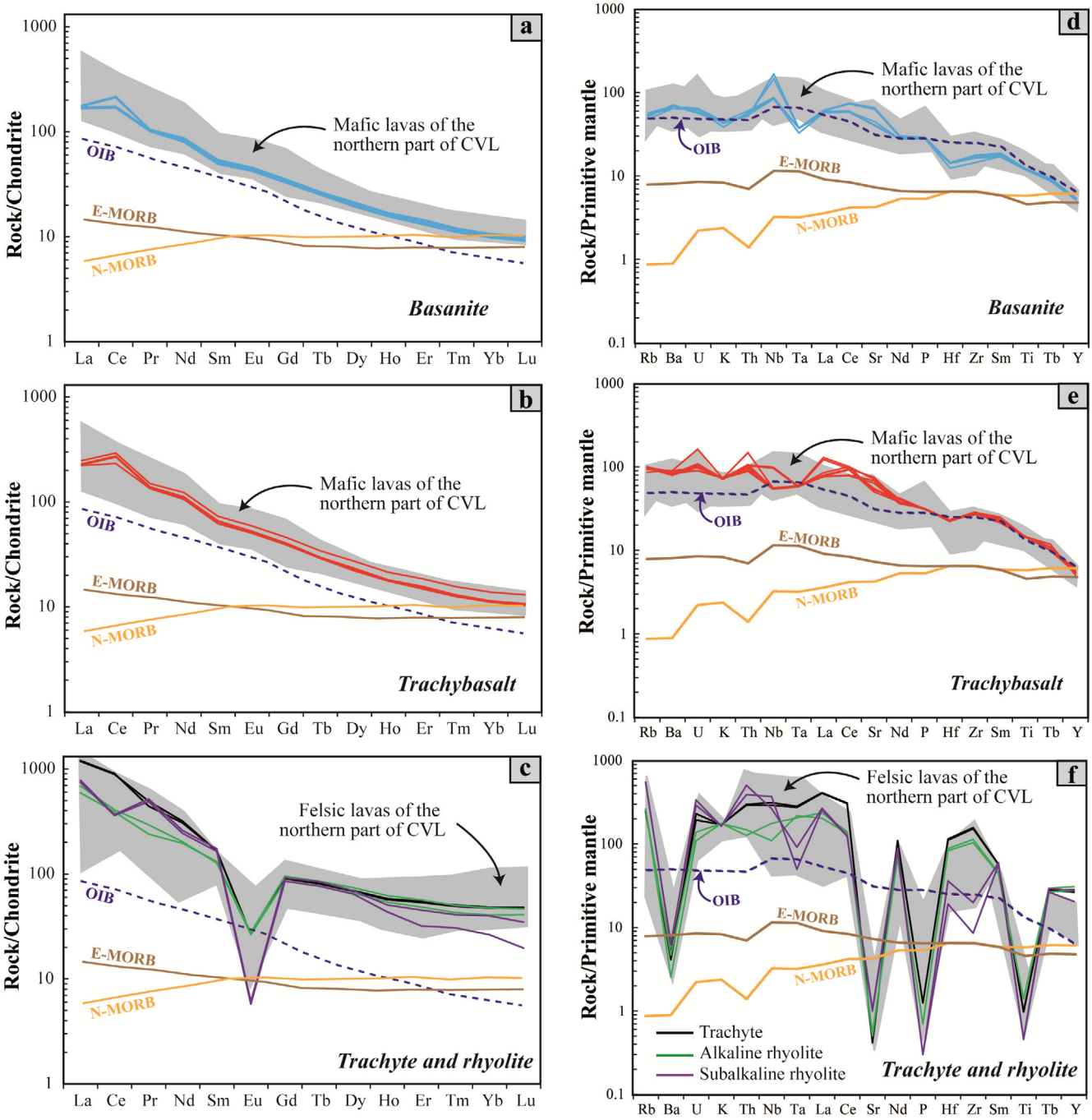

Fig. 8. (a–c) Chondrite-normalized rare earth element and (d–f) primitive-mantle normalized (after Sun and McDonough, 1989) multi-element distribution patterns for the Mokolo-Kosséhone samples. The data sources for OIB, N-MORB and E-MORB are from Sun and McDonough (1989). Data sources of the northern part of the CVL are similar to Figure 3.

Nb, La, Rb, and Zr contents with increasing silica proportions (Fig. 7e–h).

Rare earth element (REE) Chondrite-normalized presented in Figure 8a highlight negative slopes characterized by enrichment in light rare earth elements (LREEs) and depletion in heavy rare earth elements (HREEs) ($[La/Yb]_N = 12.39–32.65$, where the subscript N represents chondrite-normalized). The samples plot above Normal Mid-Ocean Ridge Basalts (N-MORB) and Enriched Mid-Ocean Ridge Basalts (E-MORB) and are very close to that of Ocean Island Basalt (OIB). This observation shows that the lavas in the study area are more enriched in REEs than N-MORB and E-MORB. The felsic lavas exhibit an important negative europium anomaly ($Eu/Eu^* = Eu_N/(Sm_N \times Gd_N)^{1/2} = 0.05–0.25$), while all the mafic samples show a slight positive Eu anomaly

(Eu/Eu* = 1.01–1.06). In the primitive mantle-normalized diagram (Sun and McDonough, 1989), Mokolo-Kosséhone samples are still similar to OIB, but with higher concentrations of trace elements, compared to those of the northern part of CVL (Fig. 8b). The profiles of the samples are more enriched in trace elements than those of N-MORB and E-MORB. Positive and negative Nb-Ta anomalies ($Nb/Nb^* = Nb_N/(Th_N \times La_N)^{1/2}$ = 0.49–2.97) are also notable.

4.2.3. Sr-Nd-Pb isotopes

Strontium (Sr), Neodymium (Nd) and Lead (Pb) isotope compositions of representative samples from Udkia and Mandaka analyzed in this study are presented in Table 1. They have the following values: $^{87}Sr/^{86}Sr$ = 0.70308–0.70378, $^{143}Nd/^{144}Nd$ = 0.51287–0.51296, $^{206}Pb/^{204}Pb$ = 19.24652–19.79122, $^{207}Pb/^{204}Pb$ = 15.70965–15.71259 and $^{208}Pb/^{204}Pb$ = 39.44921–39.86865. The isotopic values of the basaltic lavas of the study area define a line parallel to that of the basaltic lavas of the northern part of the CVL. These are generally comparable to the isotopic values of lavas of the oceanic and continental domains of the CVL (Fig. 9a, b). Like the surroundings lavas of Gawar volcano and Biu Plateau, the studied samples plot on the upper left quadrant of the bulk silicate Earth (BSE; Workman and Hart, 2005) in the $^{87}Sr/^{86}Sr$ versus $^{143}Nd/^{144}Nd$ binary diagram (Fig. 9a, c). The trend of Udkia and Mandaka lavas is parallel to the trend of the Gawar and Biu lavas (Fig. 9a–f) (south of the study area, Rankenburg et al., 2005; Gountié Dedzo et al., 2019) but with slightly lower $^{143}Nd/^{144}Nd$. Isotopic compositions of Nd for Gawar and studied samples are greater than those of Mt. Cameroon. The isotopic ratios of $^{87}Sr/^{86}Sr$ for the studied lavas and those for the northern part of CVL are comparable to those of Mt. Cameroon (0.7032–0.7036; Yokoyama et al., 2007). The lead isotopic composition of the samples commonly plots above the Northern Hemisphere Reference Line (NHRL) in the $^{206}Pb/^{204}Pb$ versus $^{207}Pb/^{204}Pb$ plot of Hart (1984; Fig. 9d).

5. DISCUSSION

5.1. Fractional Crystallization

The basanite represents the most primitive lava erupted on the Udkia volcano. It has high MgO (12.34–13.80 wt%), Cr (524.11–599.10 ppm), Co (56.93–59.66 ppm) and Ni (327.45–427.39 ppm) concentrations, and high Mg-number (Mg#: 69.40–72), consistent with a peridotite mantle origin. All other samples are characterized by low MgO (mafic: < 7.29 wt%; felsic: < 0.16 wt%), Cr (mafic: < 111.55 ppm; felsic: < 5.86 ppm), Co (mafic: < 42.32 ppm; felsic: < 2.97 ppm), Ni (mafic: < 91.72 ppm; felsic: < 5.17 ppm) and Mg# (mafic: < 60.30) values compared to melts which are in equilibrium with mantle peridotites or with a typical upper mantle mineral assemblage. These are supposed to have high values of Mg-number (68–72), and high MgO (> 10 wt%), Cr (300–500 ppm), Co (50–70 ppm) and Ni (300–400 ppm) contents (Frey et al., 1978; Jung and Masberg, 1998). Apart from the basanites, the chemical compositions of other samples from the Mokolo-Kosséhone area result from a significant effect of fractional crystallization (FC), as depicted by the trendlines observed in the major and trace elements (Figs. 6, 7, and 10a, b). For example, the constant decrease in TiO_2 and Fe_2O_{3t} (Fig. 6a, c) indicates the FC of Fe-Ti oxides. The crystallization of olivine is inferred from MgO and Ni decreasing concentrations (Figs. 6b and 7a), whereas clinopyroxene fractionation is indicated by a decrease in CaO and Sc (Figs. 6d and 7b) or Cr contents (not shown). In the advanced stages of FC, feldspar crystallization happens preferentially with an increase in the concentrations of Na_2O, K_2O, and Al_2O_3 in the mafic lavas and a decrease for the felsic ones (Fig. 6f–h). The continuous increase in Al_2O_3 throughout the differentiation process of mafic lavas demonstrates that plagioclase was not a significant crystallizing mineral phase during fractional crystallization, which is consistent with the observed slight positive Eu anomalies (1.01–1.06) (Fig. 8a, b). The decrease of Al_2O_3 throughout the FC of felsic lavas and the important negative europium anomalies (0.05–0.25) in the rhyolite and trachyte indicates the significant crystallization of plagioclase.

5.2. Crustal Contamination

During the rise of magma towards the surface in the continental domain, it can be chemically modified by the continental crust (Wigger et al., 1994). Rocks from the volcanoes in the study area are characterized by enrichment in incompatible elements, which may be due to enrichment in their mantle sources or to contamination by crustal components. Previous studies have already suggested that the contamination of primary magmas by mature and thick crust is important along the CVL (Halliday et al., 1988; Marzoli et al., 1999; Rankenburg et al., 2005; Kamgang et al., 2010; Gountié Dedzo et al., 2019). For example, this has already been demonstrated for the lavas of the volcanic province of the Kapsiki Plateau, the volcanic outpourings of Minawao and Zamay located south of the study area (Marzoli et al., 1999; Rankenburg et al., 2005; Gountié Dedzo et al., 2019).

In Figure 10c, d, a negative correlation is observed between the MgO contents and the $^{87}Sr/^{86}Sr$ isotopic ratios on the one hand, and between the SiO_2 contents and the $^{143}Nd/^{144}Nd$ isotopic ratios on the other hand. This indicates that certain basaltic lava samples from the study area were contaminated by the crust (Tchuimegnie Ngongang et al., 2015). Rankenburg et al. (2005) also recognized that Biu Plateau lavas with $^{206}Pb/^{204}Pb$ < 19.5 were

https://doi.org/10.1007/s12303-022-0030-1

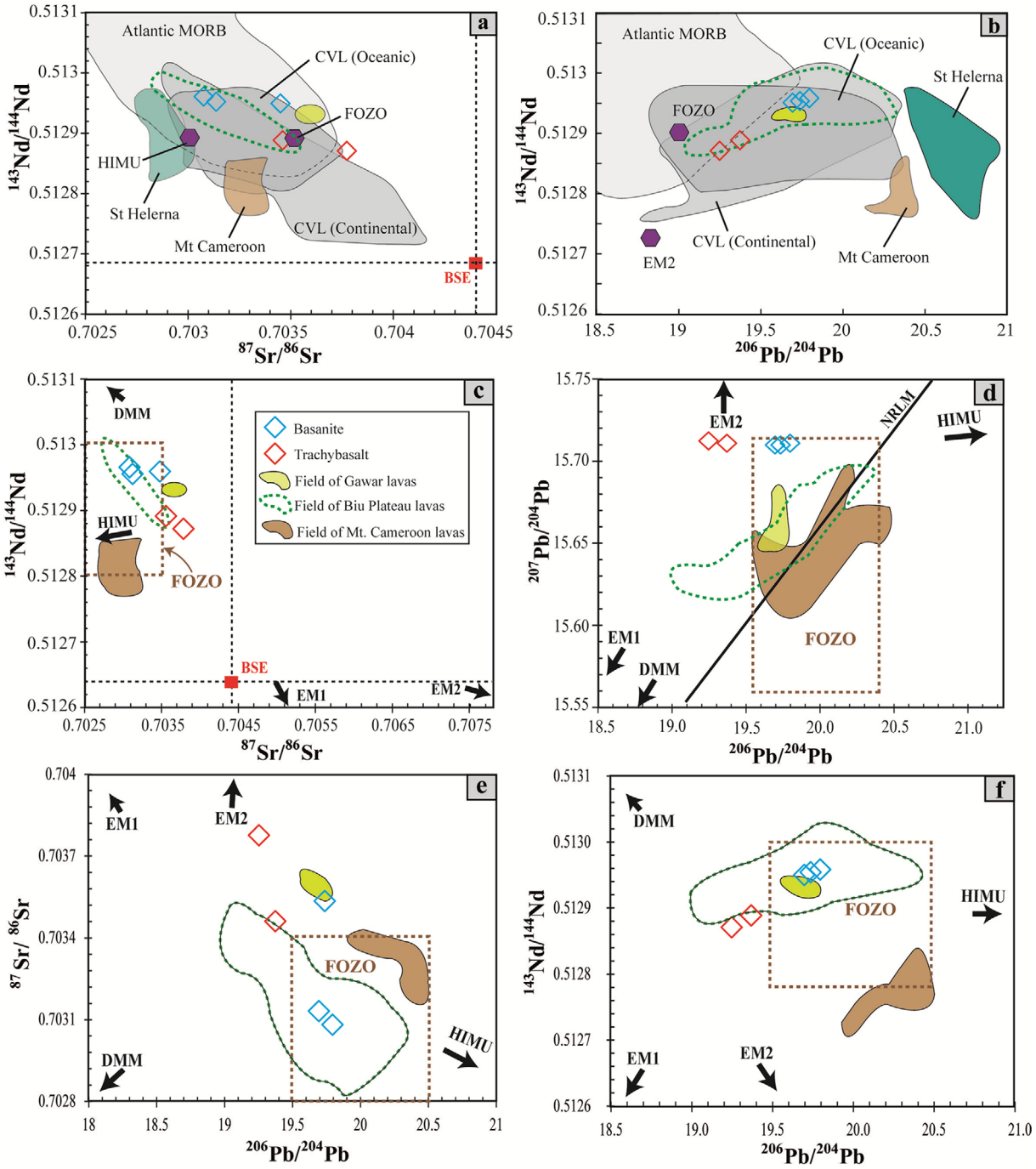

Fig. 9. (a) $^{143}Nd/^{144}Nd$ versus $^{206}Pb/^{204}Pb$ and (b) $^{143}Nd/^{144}Nd$ versus $^{206}Pb/^{204}Pb$ isotope plots of the studied lavas. FOZO and EM2 values are from Zindler and Hart (1986). Data for the CVL and Mt Cameroon are from Halliday et al. (1988), Lee et al. (1994), Ballentine et al. (1997), Marzoli et al. (2000), Rankenburg et al. (2005), Yokoyama et al. (2007), Tsafack et al. (2009), Kamgang et al. (2013). Data for the Atlantic MORB are from Meysen et al. (2007). Data for St. Helena are from Chaffey et al. (1989), Salters and White (1998) and Thirlwall (2000). (c) $^{143}Nd/^{144}Nd$ versus $^{87}Sr/^{86}Sr$ and (d) $^{207}Pb/^{204}Pb$ versus $^{206}Pb/^{204}Pb$ isotope diagrams Udkia and Mandaka lavas. Data for EM1, EM2, HIMU and DMM are from Stracke et al. (2005) and Iwamori and Nakamura (2015). Bulk Silicate Earth (BSE) after Workman and Hart (2005). Localization of FOZO is based on Stracke et al. (2005). (e) $^{87}Sr/^{86}Sr$ versus $^{206}Pb/^{204}Pb$ and (f) $^{143}Nd/^{144}Nd$ versus $^{206}Pb/^{204}Pb$ isotope plots of the studied rocks. In (c), (d), (e) and (f) data for Gawar lavas are from Gountié Dedzo et al. (2019), data for Biu Plateau are from Rankenburg et al. (2005), data for Mt Cameroon lavas are from Yokoyama et al. (2007). FOZO: Focal zone; EM: Enriched mantle; HIMU: high-μ; DMM: depleted MORB mantle.

probably contaminated by crust. Therefore, the trachybasalt samples with $^{206}Pb/^{204}Pb$ values of 19.25 and 19.37, suggest the probability of enrichment of magma with a high-μ ($^{206}Pb/^{204}Pb$ < 19.5) signature by a crustal component. The impact of this crustal contamination seems limited, as their isotopic compositions are very little modified. The influence of the crustal components on

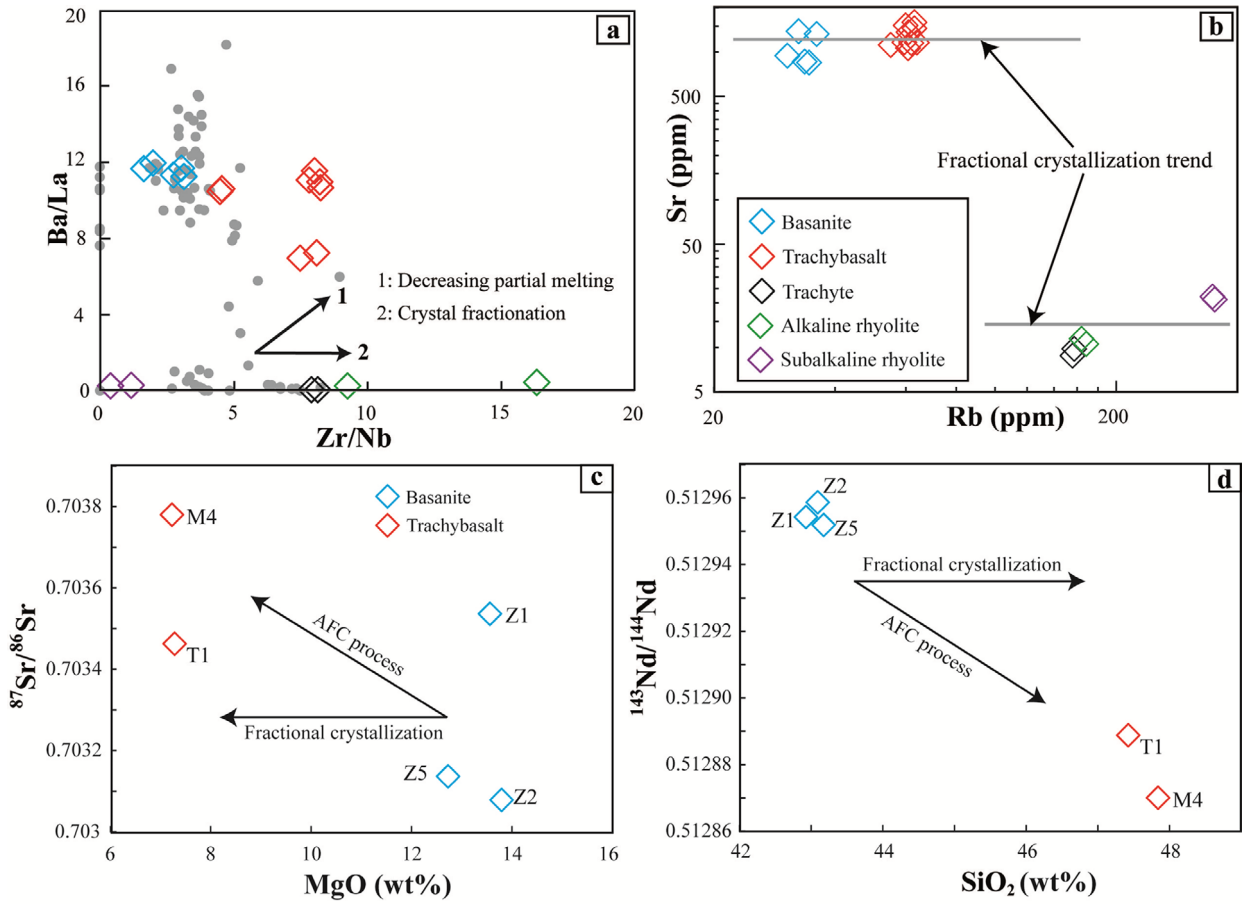

Fig. 10. (a) Ba/La versus Zr/Nb (Wendt et al., 1999) and (b) Sr versus Rb (Xu et al., 2007) diagrams showing fractional crystallization as the main petrogenetic process for the Mokolo-Kosséhone lavas. (c) $^{87}Sr/^{86}Sr$ versus MgO and (d) $^{143}Nd/^{144}Nd$ versus SiO_2 (Tchuimegnie et al., 2015) diagrams showing the contamination of some volcanic rocks in the study area.

the chemical compositions of magmas can be also determined from the different ratios of incompatible trace elements. The Rb/Y versus Nb/Y plot of Cox and Hawkesworth (1985) and Leeman and Hawkesworth (1986) is generally used to have an idea of the influence of the crustal contamination over FC on the chemical composition of the magma. In this diagram, majority of felsic rocks and trachybasalts have slightly higher Rb/Y (Table 2) ratios bringing them closer to the field of granite basement samples and thus reflecting crustal contamination (Fig. 11a). The subalkaline rhyolite S1 seems to be the most contaminated rock because it is closest to the basement samples (Fig. 11a–c). The presence of more or less significant negative Nb-Ta anomalies (Nb/Nb*: 0.49–0.89) in felsic rocks and trachybasalts on the PM-normalized diagram (Fig. 8e, f) confirms the effect of contamination during the genesis of these lavas (Zou et al., 2000).

To further constrain this effect of crustal contamination, ratios of some trace elements with a comparable degree of incompatibility (e.g., Nb/U and Ce/Pb, Table 2) were also used. The lavas have Nb/U ratios (11.51–100.77, mean: 38.23) and Ce/Pb ratios (14.16–55.10, mean: 39.91) in the same range as those found in Biu Plateau, Gawar (northern part of the CVL, mean: 50.89 and 38.84 respectively) (Rankenburg et al., 2005; Gountié Dedzo et al., 2019) and in OIB and MORB (mean: 47 ± 10 and 25 ± 5, respectively; Hofmann et al., 1986; Weaver, 1991). On the other hand, ratios of Ce/Pb and Nb/U are low for the average upper crust (4.4 and 3.7, respectively; Rudnick and Gao, 2003) and average granitic basement rocks beneath the northern part of CVL (4.13 and 3.34, respectively; Tchameni et al., 2016). The high values of these ratios in rocks from the volcanic edifices of the Mokolo-Kosséhone region preclude substantial crustal contamination. The occurrence of peridotite xenoliths included in most of the basanites and trachybasalts samples in the study area suggest the rapid ascent of magma to the surface which then minimizes the effect of crustal assimilation. This is evident in the Nb/U versus Ce/Pb (Fig. 11b) diagram where lavas from the study area plot far from a basement rock sample from the Mokong locality representing the mean composition of the granitic basement of the study area. On the Th/Yb versus Ta/Yb diagram (Fig. 11c), the lavas also plot on the mantle array typical of OIB.

https://doi.org/10.1007/s12303-022-0030-1

Table 2. Ratios of incompatible trace element of the Mokolo-Kosséhone lavas

Rock type	Sample ID	Ba/La	Zr/Nb	Nb/Y	Rb/Y	Ce/Pb	Nb/U	Th/Yb	Ta/Yb	Nb/La	Dy/Yb	La/Yb	Sm/Yb	Gd/Yb	La/Sm
Basanite	Z1	11.41	2.72	2.47	1.27	42.46	45.94	2.87	0.78	0.78	2.92	22.99	4.43	3.92	5.19
	Z2	11.48	3.08	2.56	1.48	39.53	46.14	2.79	0.92	0.92	2.96	23.75	4.54	4.03	5.24
	Z3	11.63	1.63	4.88	1.48	55.10	100.77	2.61	0.89	0.89	3.05	24.19	4.72	4.12	5.12
	Z4	11.79	1.93	4.19	1.32	53.37	85.15	2.53	0.85	0.85	2.98	23.31	4.58	3.99	5.09
	Z5	11.64	3.01	2.51	1.36	40.54	45.88	2.89	0.85	0.85	2.88	22.83	4.36	3.85	5.24
Trachybasalt	M1	10.76	8.09	1.72	2.40	24.03	11.51	5.37	1.03	1.03	2.94	25.02	4.75	4.01	5.26
	M2	10.72	8.18	1.56	2.43	29.51	17.12	4.72	1.27	1.27	3.04	28.00	5.16	4.21	5.42
	M3	11.16	8.03	1.57	2.36	32.26	18.59	4.51	1.29	1.29	3.05	28.98	5.31	4.29	5.46
	M4	10.54	4.49	2.56	2.34	26.57	33.16	4.67	1.26	1.26	2.97	28.06	5.02	4.24	5.59
	M5	10.94	7.90	1.57	2.43	30.20	21.05	4.08	1.25	1.25	3.04	27.82	5.22	4.25	5.33
	M6	10.82	8.14	1.57	2.53	30.38	18.91	4.40	1.27	1.27	3.06	27.84	5.21	4.29	5.34
	T1	10.58	4.52	2.54	2.19	25.92	32.04	4.74	1.28	1.28	2.97	27.73	5.04	4.23	5.50
	T2	7.25	8.10	1.57	2.57	31.82	20.31	4.07	1.27	1.27	3.08	45.52	5.35	4.30	8.51
	T2	7.06	7.51	1.66	2.49	30.97	19.47	3.97	1.18	1.18	3.07	43.15	5.18	4.29	8.33
Trachyte	U1	0.10	7.89	1.73	1.22	49.63	46.10	3.08	1.41	1.41	2.16	34.31	3.08	2.36	11.13
	U2	0.12	8.18	1.73	1.29	50.94	51.13	3.07	1.40	1.40	2.18	34.53	3.14	2.31	11.00
Alkaline rhyolite	L1	0.23	16.32	0.55	1.16	26.75	26.83	1.56	1.10	1.10	2.34	17.27	2.48	2.43	6.95
	L2	0.11	9.24	1.00	1.34	29.01	54.70	1.54	1.21	1.21	2.40	23.26	2.79	2.53	8.33
Subalkaline rhyolite	S1	0.24	1.18	1.50	2.75	15.15	26.72	6.29	0.55	0.55	2.60	26.96	3.90	2.78	6.92
	S3	0.26	0.36	2.83	3.76	14.16	43.15	7.35	0.45	0.45	3.63	38.87	5.57	3.90	6.98
CVL lavas (Northern part)	–	0.09–18.16	0.00–8.96	0.35–7.50	0.04–5.76	26.80–58.58	6.76–78.46	1.79–10.50	0.26–7.56	0.20–2.83	1.20–3.72	2.25–49.09	3.50–5.00	2.13–5.85	3.59–5.35
Precambrian basement	–	–	–	0.21–0.62	2.55–8.53	1.40–7.84	1.11–6.09	4.78–50.92	0.58–1.18	–	–	–	–	–	–

Data sources of the northern part of the CVL are from Marzoli et al. (1999, 2000), Ngounouno et al. (2000), Rankenburg et al. (2005), Gountié Dedzo et al. (2019). Data for Precambrian basement are from Tchameni et al. (2016).

5.3. Partial Melting, Depth Estimation and Nature of the Sources

The geochemical features of the lavas as discussed above indicate that FC was the principal differentiation process with contamination playing a limited role. The chemical compositions of the mantle source can be identified by particular incompatible elements ratios (e.g., Zr/Hf, Th/U, Nb/Ta, La/Ce, Nb/U). The lavas from the same source present approximately similar values of these ratios. The ratios of Zr/Hf, Th/U, Nb/Ta, La/Ce and Nb/U of the mafic lavas (41.97–45.44, 3.58–4.23, 16.07–40.66, 0.32–0.50 and 17.12–45.94, respectively) are comparable to those of the felsic lavas (45.33–49.69, 4.34–6.08, 14.93–50.41, 0.51–0.82 and 26.72–46.1, respectively), signifying that both series are co-genetic.

The Precambrian granitic basement rocks from Mokong have high ratios of some incompatible trace elements (LILE/HFSE) such as Th/Ta, Ba/Nb, Rb/Nb, and Rb/Zr (6.23–88.12, 49.39–159.83, 4.13–36.04 and 0.33–1.37, respectively) compared to those of the mafic and felsic lavas (1.41–5.21, 0.13–16.00, 0.30–2.10 and 0.09–0.20, respectively) in the study area precluding an origin from direct crustal melting (Kwékam et al., 2015). The lavas of the Mokolo-Kosséhone region could therefore have a mantle origin. The $(Ce/Pb)_N$ ratios (1.06–2.20) of the study lavas are > 1, which characterize plume-derived magmas (Tian et al., 2010).

The enrichment in LREE over HREE along with $(La/Yb)_N > 5$ (12.39–32.65), $(Tb/Yb)_N > 1.7$ (1.71–2.89) (Fig. 12a) and Dy/Yb > 2 (2.16–3.63) (Fig. 12b), suggest a mantle source with the presence of a garnet phase (Wang et al., 2002; Jung et al., 2006). The variation diagrams for Sm/Yb versus La/Sm (Fig. 13a) and that of Gd/Yb versus La/Yb (Fig. 13b), confirm the presence of residual garnet in the source of the Mokolo-Kosséhone lavas. These diagrams show that the samples and other lavas of the northern part of CVL resulted from a low degree of partial melting (< 4%) of a source containing less than 5% of garnet peridotite. These amounts of garnet in the source and degree of partial melting are also comparable with those described in the earlier studies of the CVL (Asaah et al., 2015a).

To estimate the lithospheric thickness and depth of melting, trace elements in basaltic lavas are good parameters (McKenzie and O'nions, 1991; Mattey et al., 1994; Putirka, 1999; Zheng et

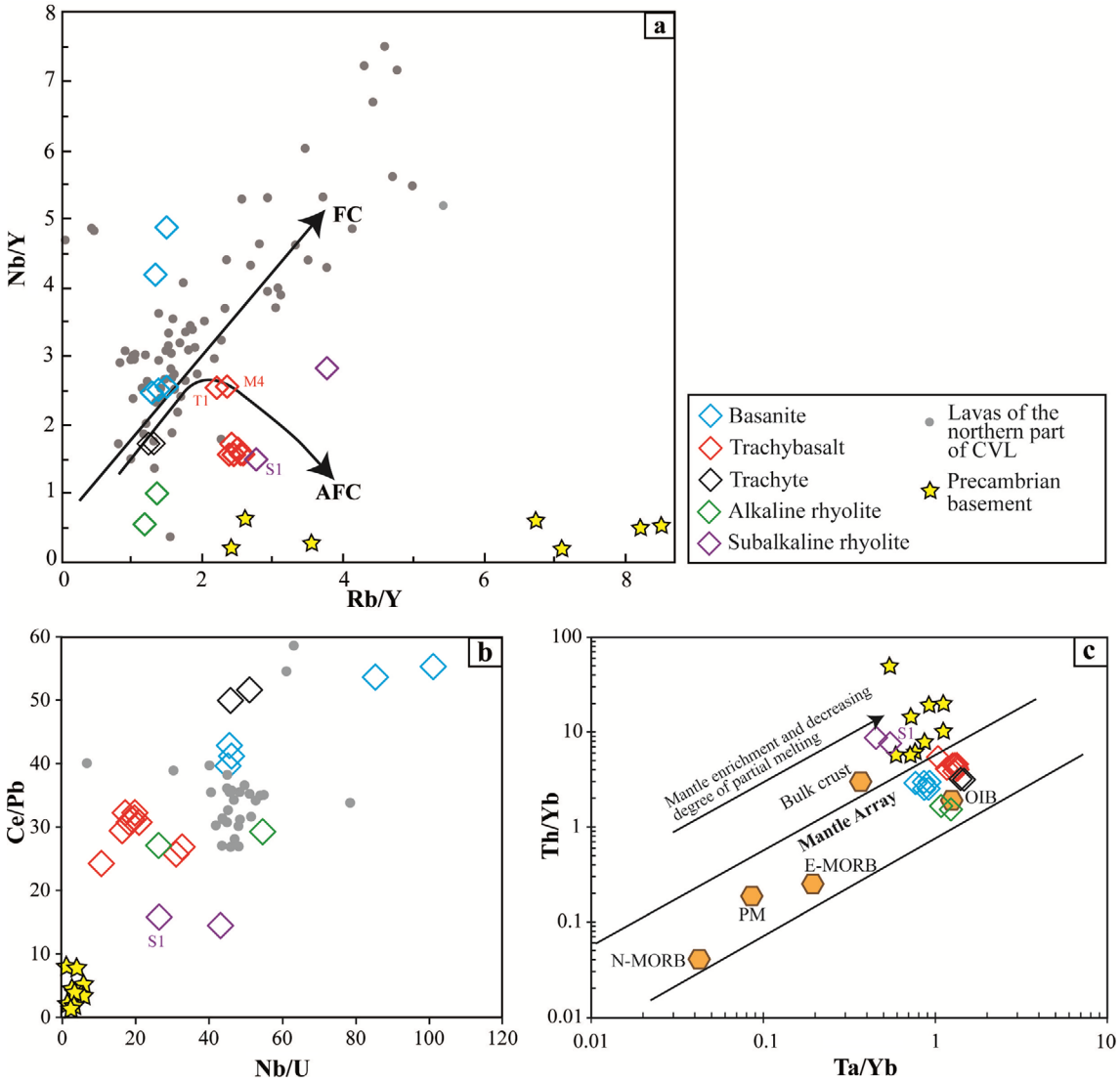

Fig. 11. (a) Plot of Nb/Y versus Rb/Y (Cox and Hawkesworth, 1985; Leeman and Hawkesworth, 1986) showing basement samples relative to the Mokolo-Kosséhone lavas and the lavas of the northern part of CVL. (b) Nb/U versus Ce/Pb diagram after Asaah et al. (2020). Data for Precambrian basement are from Tchameni et al. (2016). (c) Diagram of Th/Yb versus Ta/Yb illustrating that the Mokolo-Kosséhone lavas plot on the mantle array typical of OIB.

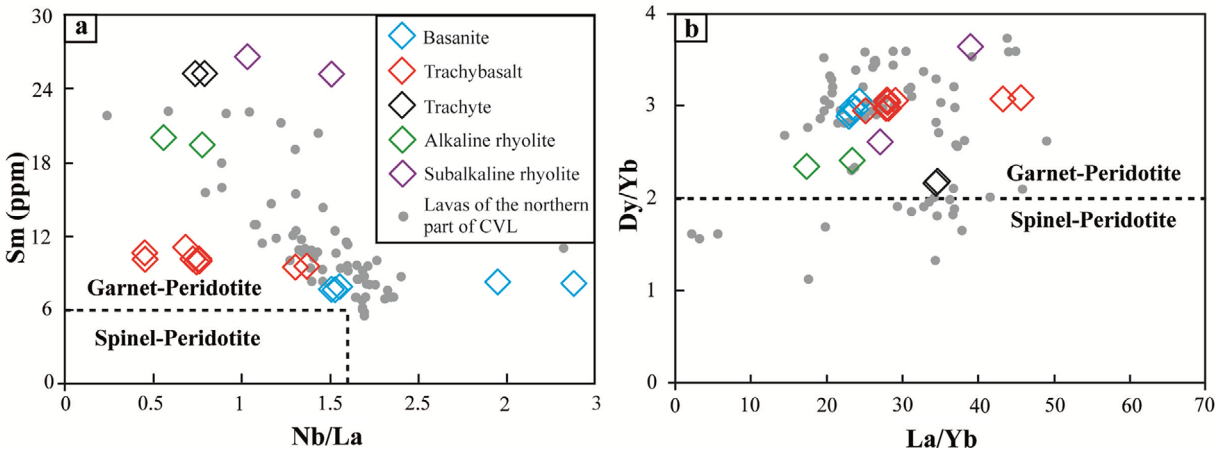

Fig. 12. (a) Diagrams of Sm versus Nb/La and (b) Dy/Yb versus La/Yb (Jung et al., 2006) showing the garnet-peridotite source for the Mokolo-Kosséhone rocks and others lavas of the northern part of CVL.

https://doi.org/10.1007/s12303-022-0030-1

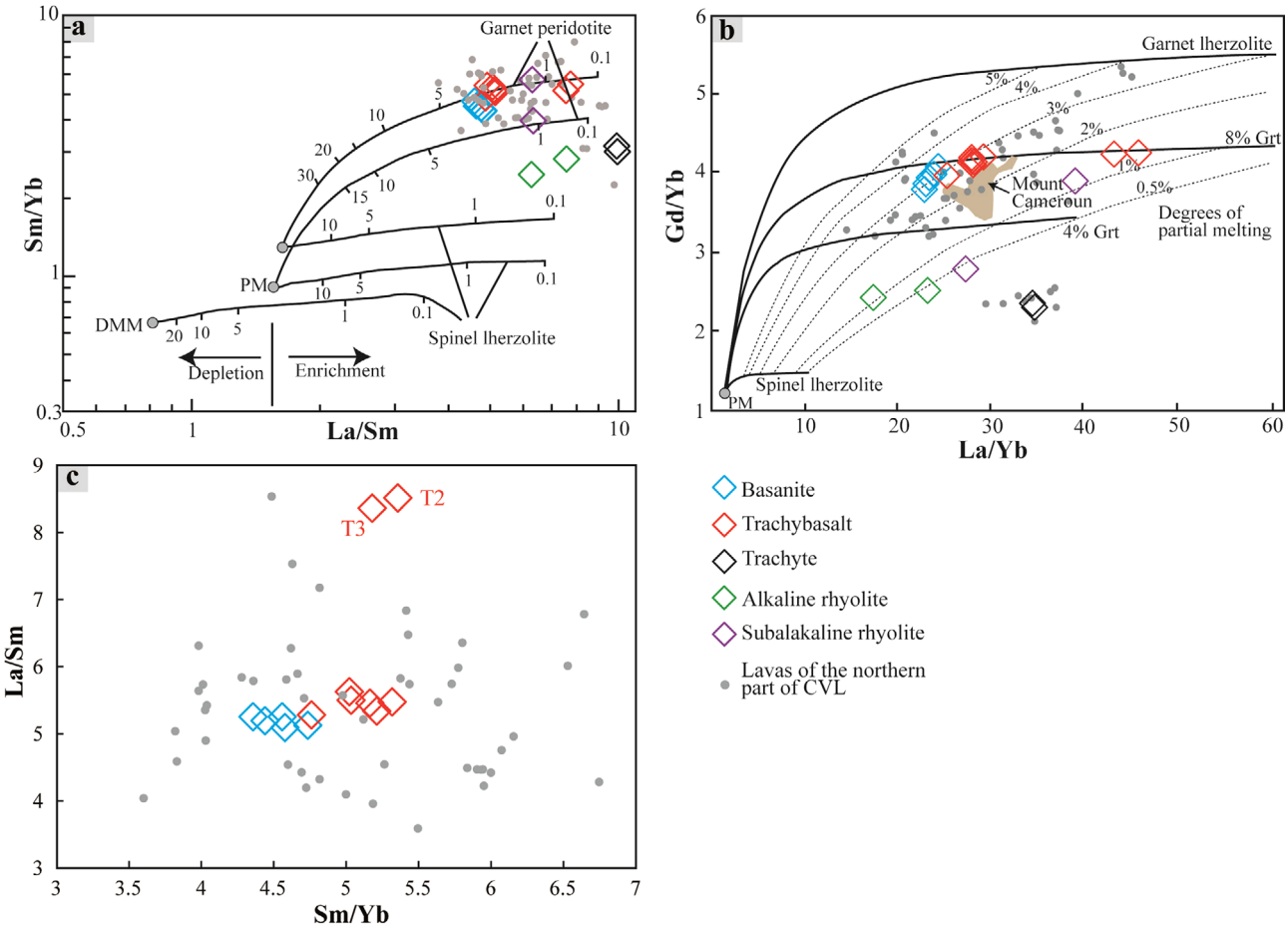

Fig. 13. (a) Plot of the Mokolo-Kosséhone lavas in the Sm/Yb versus La/Sm diagram after Gurenko et al. (2006). Values of DMM (Depleted MORB Mantle) are from Workman and Hart (2005). Values of PM (Primitive Mantle) are from Sun and McDonough (1989). The different curves represent the partial melting of garnet and spinel peridotites. The gradations represent the different fusion rates. (b) Illustration of partial melting for Mokolo-Kosséhone lavas in Gd/Yb versus La/Yb diagram after Yokoyama et al. (2007). The two curves marked Grt 4% and 8% represent the garnet contents of the source. Calculations of the garnet contents of the source were made using the partition coefficients of Halliday et al. (1995). (c) Sm/Yb versus La/Sm plot after Asaah et al. (2020) showing relative depth of source melting of mafic lavas.

al., 2003). The low of Ce/Yb ratios of basanite from Udkia (59.6–75.5; mean: 66.1) suggest that their magma formed at shallow levels with respect to the trachybasalts from Mandaka and Ouro Tada that have high Ce/Yb values (Mandaka: 75.36–88.97, mean: 82.76; and Ouro Tada: 73.91–91.43; mean: 84.04). This is concordant with the La/Sm versus Sm/Yb plot (Fig. 13c) that shows Mandaka and Ouro Tada lavas plotting at higher values of La/Sm and Sm/Yb. It is important to note that two trachybasalts samples (T2 and T3) from Ouro Tada have very high values of Sm/Yb and La/Sm, signifying that the magma was sampled at a greater depth compared to the other Ouro Tada samples.

Focal zone (FOZO), depleted mantle (DM), enriched mantle (EM), and high-μ (HIMU) are the different mantle reservoirs identifiable based on the Sr-Nd-Pb isotope systematics of OIB-like basalts (Lustrino and Dallai, 2003; Stracke et al., 2005; Willbold and Stracke, 2006, 2010). This approach is frequently applied nowadays to intra-plate continental settings (Chung et al., 1995; Milner and Le Roex, 1996; Lustrino, 2005). According to Asaah et al. (2015a), DM, FOZO, and an enrichment component are involved in the magmatism of the CVL. All the samples plotted in the isotope diagrams overlap with the fields of the Gawar and Biu Plateau lavas, predominantly near the FOZO (Fig. 9a–f). Trace elements and Sr and Nd isotopic compositions of the Mokolo-Kosséhone lavas are consistent with a mixture of different source materials from the sub-continental lithospheric mantle (SCLM) and the asthenosphere with minor crustal contamination. The source composition is analogous to those described in the northern portion of the CVL (Rankenburg et al., 2005; Gountié Dedzo et al., 2019) and other volcanic massifs along the CVL (e.g., Marzoli et al., 2000; Déruelle et al., 2007; Tamen et al., 2007; Yokoyama et al., 2007; Aka et al., 2008; Kamgang et al., 2013; Asaah et al., 2015a, 2015b, 2020, 2021; Tchuimegnie et al., 2015).

6. CONCLUSIONS

The Mokolo-Kosséhone samples range from mafic (basanite, trachybasalt) to felsic rocks (trachyte, alkaline, and subalkaline rhyolites) similar to most of the rocks of the northern part of the CVL. Except for the subalkaline rhyolites (two samples), all the other eighteen samples show alkaline affinity. The fluctuations in major element oxides and compatible trace elements contents from basanite to rhyolite can be attributed to the fractional crystallization of various mineral phases such as olivine, clinopyroxene, amphibole, plagioclase, sanidine, biotite, and oxides. Ratios of trace elements (Nb/U and Ce/Pb), and Sr-Nd-Pb isotopic data of the mafic lavas compared to those of the Mokong granite, OIB and MORB indicate minor crustal contamination. The enrichment in LREEs and depletion in HREEs associated with $(La/Yb)_N > 5$, $(Tb/Yb)_N > 1.7$, and $Dy/Yb > 2$, suggest the presence of a garnet phase in the mantle source. Geochemical modeling also show that the lavas were produced at varying depths by low degree of partial melting (< 4%) of a source containing less than 5% of garnet peridotite. Trace element and isotopic compositions of the Mokolo-Kosséhone lavas are consistent with a mixture of different source materials from the sub-continental lithospheric mantle and the asthenosphere with minor crustal contamination.

ACKNOWLEDGMENTS

This paper is a part of the first author's PhD thesis in preparation. We would like to thank anonymous reviewers and Associate editor, Ian Ernest Smith, for critically reading the manuscript and suggesting substantial improvements.

REFERENCES

Asaah, A.N.E., Yokoyama, T., Aka F.T., Iwamoria, H., Kuritani, T., Usuia, T., Gountié Dedzo, M., Tamen, J., Hassegawa, T., Fozing, E.M., Wirmvem, M.J., and Nche, A.L., 2020, Major/trace elements and Sr-Nd-Pb isotope systematics of lavas from lakes Barombi Mbo and Barombi Koto in the Kumba graben, Cameroon Volcanic Line: constraints on petrogenesis. Journal of African Earth Sciences, 161, 103675.

Asaah, A.N.E., Yokoyama, T., Aka, F.T., Usui, T., Kuritani, T., Wirmvem, M.J., Iwamori, H., Fozing, E.M., Tamen, J., Mofor, G.Z., Ohba, T., Tanyileke, G., and Hell, J.V., 2015b, Geochemistry of lavas from maar-bearing volcanoes in the Oku Volcanic Group of the Cameroon Volcanic Line. Chemical Geology, 406, 55–69.

Asaah, A.N.E., Yokoyama, T., Aka, F.T., Usui, T., Wirmvem, M.J., Chako Tchamabé, B., Ohba, T., Tanyileke, G., and Hell, J.V., 2015a, A comparative review of petrogenetic processes beneath the Cameroon Volcanic Line: geochemical constraints. Geosciences Frontiers, 6, 557–570.

Asaah, A.N.E., Yokoyama, T., Iwamori, H., Aka, F.T., Kuritani, T., Usui, T., Tamen, J., Gountié Dedzo, M., Chako Tchamabé, B., Hasegawa, T., Nche, L.A., and Ohba, T., 2021, High-μ signature in lavas of Mt. Oku: implications for lithospheric and asthenospheric contributions to the magmatism of the Cameroon Volcanic Line (West Africa). Lithos, 400–401, 106416.

Ballentine, C.J., Lee, D.-C., and Halliday, A.N., 1997, Hafnium isotopic studies of the Cameroon line and new HIMU paradoxes. Chemical Geology, 139, 111–124.

Barfod, D.N., Ballentine, C.J., Halliday, A.N., and Fitton, J.G., 1999, Noble gases in the Cameroon line and the He, Ne, and Ar isotopic compositions of high μ (HIMU) mantle. Journal of Geophysical Research, Solid Earth, 104, 29509–29527.

Chaffey, D.J., Cliff, R.A., and Wilson, B.M., 1989, Characterization of the St. Helena magma source magmatism in the ocean basins. In: Saunders, A.D. and Norry, M.J. (eds.), Magmatism in the Ocean Basins. Geological Society, London, Special Publications, 42, p. 257–276. https://doi.org/10.1144/GSL.SP.1989.042.01.16

Chung, S.L., Jahn, B.M., Chen, S.J., Lee, T., and Chen, C.H., 1995, Miocene basalts in northwestern Taiwan: evidence for EM-type mantle sources in the continental lithosphere. Geochimica et Cosmochimica Acta, 59, 549–555.

Cox, K.G. and Hawkesworth, C.J., 1985, Geochemical stratigraphy of the Deccan Traps at Mahabaleshwar, western Ghats, India, with implications for open system magmatic processes. Journal of Petrology, 26, 355–377.

Déruelle, B., Ngounouno, I., and Demaiffe, D., 2007, The "Cameroon Hot Line" (CHL): a unique example of active alkaline intraplate structure in both oceanic and continental lithospheres. Comptes Rendus Geoscience, 339, 589–600.

Fitton, J.G., and Dunlop, H.M., 1985, The Cameroon line, West Africa, and its bearing on the origin of oceanic and continental alkali basalt. Earth and Planetary Science Letters, 72, 23–38.

Fosso, J., Ménard, J.J., Bardintzeff, J.M., Wandji, P., Tchoua, F.M., and Bellon, H., 2005, Les laves du mont Bangou: une première manifestation volcanique éocène, à affinité transitionnelle, de la Ligne du Cameroun. Comptes Rendus de l'Académie des Sciences, 337, 315–325.

Frey, F.A., Green, D.H., and Roy, S.D., 1978, Integrated models of basalt petrogenesis: a study of quartz tholeiites to olivine melilitites from South Eastern Australia utilizing geochemical and experimental petrological data. Journal of Petrology, 19, 463–513.

Gountié Dedzo, M., Asaah, A.N.E., Fozing, E.M., Tchamabé, B.C., Tefogoum Zangmo, G., Dagwai, N., Tchokona Seuwui, D., Kamgang, P., Aka, F.T., and Ohba, T., 2019, Petrology and geochemistry of lavas from Gawar, Minawao and Zamay volcanoes of the northern segment of the Cameroon Volcanic Line (central Africa): constraints on mantle source and geochemical evolution. Journal of African Earth Sciences, 153, 31–41.

Gountié Dedzo, M., Diddi Hamadjoda, D., Martial Fozing, E., Tchamabé, B.C., Mendoza Rosas, A.T., Asaah, A.N.E., Tefogoum Zangmo, G., Kamgang, P., and Ohba, T., 2020, Petrology and geochemistry of ignimbrites and associated enclaves from Mount Bambouto, West-Cameroon, Cameroon Volcanic Line. Geochemistry, 80, 125663. https://doi.org/10.1016/j.chemer.2020.125663

Gountié Dedzo, M, Fozing, E.M., Chako-Tchamabé, B., Biakan à

Nyotok, P.C., Diddi Hamadjoda, D., Asaah, A.N.E., Zangmo Tefogoum, G., Kamgang, P., and Ohba, T., 2022, Geochemical features and petrology of ignimbrites deposits from Bamenda volcano, western Highlands of the Cameroon Volcanic Line. Arabian Journal of Geosciences, 15, 643.

Grant, N.K., Rex, D.C., and Freeth, S.J., 1972, Potassium-argon ages and strontium isotope ratio measurements from volcanic rocks in northeastern Nigeria. Contributions to Mineralogy and Petrology, 35, 277–292.

Gurenko, A., Hoernle, K., Hauff, F., Schmincke, H., Han, D., Miura, Y., and Kaneoka, I., 2006, Major, trace element and Nd-Sr-Pb-O-He-Ar isotope signatures of shield stage lavas from the central and western Canary Islands: insights into mantle and crustal processes. Chemical Geology, 233, 75–112.

Halliday, A.N., Dickin, A.P., Fallick, A.E., and Fitton, J.G., 1988, Mantle dynamics: a Nd, Sr, Pb and O isotopic study of the Cameroon Line volcanic chain. Journal of Petrology, 29, 181–211.

Halliday, A.N., Lee, D.C., Tommasini, S., Davies, G.R., Paslick, C.R., Fitton, J.G., and James, D.E., 1995, Incompatible trace elements in OIB and MORB and source enrichment in the sub oceanic mantle. Earth and Planetary Science Letters, 133, 379–395.

Hamelin, B., Manhes, G., Albarede, F., and Allegre, C.J., 1985, Precise lead isotope measurements by the double spike technique: a reconsideration. Geochimica et Cosmochimica Acta, 49, 173–182.

Hofmann, A.W., Jochum, K.P., Seufert, M., and White, W.M., 1986, Nb and Pb in oceanic basalts: new constraints on mantle evolution. Earth and Planetary Science Letters, 79, 33–45.

Irvine, T.N. and Baragar, W.R.A., 1971, A guide to the chemical classification of the common volcanic rocks. Canadian Journal of Earth Sciences, 8, 523–548.

Itiga, Z., Bardintzeff, J.M., Wotchoko, P., Wandji, P., and Bellon, H., 2013, Tchabal Gangdaba massif in the Cameroon Volcanic Line: a bimodal association. Arabian Journal of Geosciences, 7, 4641–4664.

Iwamori, H. and Nakamura, H., 2015, Isotopic heterogeneity of oceanic, arc and continental basalts and its implications for mantle dynamics. Gondwana Research, 27, 1131–1152.

Jung, C., Jung, S., Hoffer, E., and Berndt, J., 2006, Petrogenesis of Tertiary mafic alkaline magmas in the Hocheifel, Germany. Journal of Petrology, 47, 1637–1671.

Jung, S. and Masberg, P., 1998, Major- and trace-element systematics and isotope geochemistry of Cenozoic mafic volcanic rocks from the Vogelsberg (central Germany): constraints on the origin of continental alkaline and tholeiitic basalts and their mantle sources. Journal of Volcanology and Geothermal Research, 86, 151–177.

Kamgang, P., Chazot, G., Njonfang, E., Tchuimegnie Ngongang, N.B., and Tchoua, F., 2013, Mantle sources and magma evolution beneath the Cameroon Volcanic Line: geochemistry of mafic rocks from the Bamenda Mountains (NW Cameroon). Gondwana Research, 24, 727–741.

Kamgang, P., Njonfang, E., Nono, A., Dedzo, M.G., and Tchoua, F.M., 2010, Petrogenesis of a silicic magma system: geochemical evidence from Bamenda Mountains, NW Cameroon, Cameroon Volcanic Line. Journal of African Earth Sciences, 58, 285–304.

Kuritani, T. and Nakamura, E., 2003, Highly precise and accurate isotopic analysis of small amounts of Pb using ^{205}Pb-^{204}Pb and ^{207}Pb-^{204}Pb, two double spikes. Journal of Analytical Atomic Spectrometry, 18, 1464–1470.

Kwékam, M., Liégeois, J.P., Njonfang, E., Affaton, P., Hartmann, G., and Tchoua, F., 2010, Nature origin and significance of the Pan-African high-K calc-alkaline Fomopéa plutonic complex in the Central African fold belt (Cameroon). Journal of African Earth Sciences, 57, 79–95.

Le Bas, M.J., Le Maitre, R.N., Streckeisen, A., and Zanettin, B., 1986, A chemical classification of volcanic rock based on total silica diagram. Journal of Petrology, 27, 745–750.

Le Maitre, R.W., 2002, Igneous Rocks: A Classification and Glossary of Terms. Recommendations of the International Union of Geological Sciences Subcommission on the Systematics of Igneous Rocks, Cambridge, 236 p.

Lee, D.C., Halliday, A.N., Fitton, G.J., and Poli, G., 1994, Isotopic variations with distance and time in the volcanic islands of the Cameroon Line: evidence of the mantle plume origin. Earth and Planetary Science Letters, 123, 119–138.

Leeman, W.P. and Hawkesworth, C.J., 1986, Open magma systems: trace element and isotopic constraints. Journal of Geophysical Research, 91, 5901–5912.

Letterman, M., 1984, Regional geological study of Anloua basin (Cameroon). Ph.D. Thesis, University of Orléans, Orléans, 194 p.

Lustrino, M., 2005, How the delamination and detachment of the lower crust can influence basaltic magmatism. Earth-Science Reviews, 72, 21–38.

Lustrino, M. and Dallai, L., 2003, On the origin of EM-I end-member. Neues Jahrbuch für Mineralogie - Abhandlungen, 179, 85–100.

Makishima, A., Nakamura, E., and Nakano, T., 1999, Determination of zirconium, niobium, hafnium and tantalum at ng g-1 levels in geological materials by direct nebulisation of sample HF solution into FI-ICP-MS. Geostandard Newsletter, 23, 7–20.

Marzoli, A., Piccirillo, E.M., Renne, P.R., Bellieni, G., Iacumin, M., Nyobe, J.B., and Tongwa, A.T., 2000, The Cameroon Volcanic Line revisited: petrogenesis of continental basaltic magmas from lithospheric and asthenospheric mantle sources. Journal of Petrology, 41, 87–109.

Marzoli, A., Renne, P.R., Piccirillo, E.M., Castorina, F., Bellieni, G., Melfi, A.J., Nyobe, J.B., and N'ni, J., 1999, Silicic magmas from the continental Cameroon Volcanic Line (Oku, Bambouto and Ngaoundere): ^{40}Ar-^{39}Ar dates, petrology, Sr-Nd-O isotopes and their petrogenetic significance. Contributions to Mineralogy and Petrology, 135, 133–150.

Mattey, D.P., Lowry, D., and Macpherson, C., 1994, Oxygen isotope composition of mantle peridotite. Earth and Planetary Science Letters, 128, 231–241.

McKenzie, D. and O'nions, R.K., 1991, Partial melt distributions from inversion of rare earth element concentrations. Journal of Petrology, 32, 1021–1091.

Meysen, C.M., Blichert-Toft, J., Ludden, J.N., Humler, E., Mével, C., and Albarède, F., 2007, Isotopic portrayal of the Earth's upper mantle flow field. Nature, 447, 1069–1074.

Middlemost, E.A.K., 1975, The basalt clan. Earth Sciences Reviews, 11, 337–364.

Milner, S.C. and Le Roex, A.P., 1996, Isotope characteristics of the

Okenyenya igneous complex, northwestern Namibia: constraints on the composition of the early Tristan plume and the origin of the EM1 mantle component. Earth and Planetary Science Letters, 141, 277–291.

Moundi, A., Wandji, P., Bardintzeff, J.-M., Ménard, J.J., Okomo Atouba, L.C., Mouncherou, O.F., Reusser, É., Bellon, H., and Tchoua, F.M., 2007, Les basaltes éocènes à affinité transitionnelle du plateau Bamoun, témoins d'un réservoir mantellique enrichi sous la ligne volcanique du Cameroun. Comptes Rendus Geoscience, 339, 396–406.

Ngounouno, I., Déruelle, B., and Demaiffe, D., 2000, Petrology of the bimodal Cenozoic volcanism of the Kapsiki plateau (Northermost Cameroon, central Africa). Journal of Volcanology and Geothermal Research, 102, 21–44.

Njome, M.S. and de Wit, M.J., 2014, The Cameroon Line: analysis of an intraplate magmatic province transecting both oceanic and continental lithospheres: constraints, controversies and models. Earth-Science Reviews, 139, 168–194.

Nkouandou, O.F., Ngounouno, I., Déruelle, B., Ohnenstetter, D., Montigny, R., and Demaiffe, D., 2008, Petrology of the Mio-Pliocene volcanism to the North and East of Ngaoundéré (Adamawa, Cameroon). Comptes Rendus Geoscience, 340, 28–37.

Nono, A., Déruelle, B., Demaiffe, D., and Kambou, R., 1994, Tchabal Nganha volcano in Adamawa (Cameroon): petrology of a continental alkaline lava series. Journal of Volcanology and Geothermal Research, 60, 147–178.

Putirka, K., 1999, Melting depths and mantle heterogeneity beneath Hawaii and the east Pacific rise: constraints from Na/Ti and REE ratios. Journal of Geophysical Research, 104, 2817–2829.

Rankenburg, K., Lassiter, J.C., and Brey, G., 2005, The role of continental crust and lithospheric mantle in the genesis of Cameroon Volcanic Line lavas: constraints from isotopic variations in lavas and megacrysts from the Biu and Jos Plateaux. Journal of Petrology, 46, 169–190.

Rudge, J.F., Reynolds, B.C., and Bourdon, B., 2009, The double spike toolbox. Chemical Geology, 265, 420–431.

Rudnick, R.L. and Gao, S., 2003, Composition of the continental crust. In: Holland, H.D. and Turekian, K.K. (eds.), Treaties on Geochemistry: The Crust. Elsevier, 3, p. 1–64. https://doi.org/10.1016/b0-08-043751-6/03016-4

Salters, V.J.M. and White, W.M., 1998, Hf isotope constraints on mantle evolution. Chemical Geology, 145, 447–460.

Salzmann, U., 2000, Are modern savannas degraded forests? – A Holocene pollen record from the Sudanian vegetation zone of NE Nigeria. Vegetation History and Archaeobotany, 9, 1–15.

Sato, H., Aramaki, S., Kusakabe, M., Hirabayashi, J., Sano, Y., Nojiri, Y., and Tchoua, F., 1990, Geochemical difference of basalts between polygenetic and monogenetic volcanoes in the central part of the Cameroon volcanic line. Geochemical Journal, 24, 357–370.

Stracke, A., Hofmann, A.W., and Hart, S.R., 2005, FOZO, HIMU, and the rest of the mantle zoo. Geochemistry, Geophysics, Geosysems, 6, 1–20.

Suh, C.E., Sparks, R.S.J., Fitton, J.G., Ayonghe, S.N., Annen, C., Nana, R., and Luckman, A., 2003, The 1999 and 2000 eruptions of Mount Cameroon: eruption behaviour and petrochemistry of lava. Bulletin of Volcanology, 65, 267–281.

Sun, S.-S. and McDonough, W., 1989, Chemical and isotopic systematics of oceanic basalts: implications for mantle composition and processes. In: Saunders, A.D. and Norry, M.J. (eds.), Magmatism in the Ocean Basins. Geological Society, London, Special Publications, 42, p. 313–345. https://doi.org/10.1144/GSL.SP.1989.042.01.19

Tamen, J., Nkoumbou, C., Mouafo, L., Reusser, E., and Tchoua, F.M., 2007, Petrology and geochemistry of monogenetic volcanoes of the Barombi Koto volcanic field (Kumba graben, Cameroon volcanic line): implications for mantle source characteristics. Comptes Rendus Geosciences, 339, 799–809.

Tamen, J., Nkoumbou, C., Reusser, E., and Tchoua, F., 2015, Petrology and geochemistry of mantle xenoliths from the Kapsiki plateau (Cameroon volcanic line): implications for lithospheric upwelling. Journal of African Earth Sciences, 101, 119–134.

Tanaka, T., Togashi, S., Kamioka, H., Amakawa, H., Kagami, H., Hamamoto, T., Yuhara, M., Orihashi, Y., Yoneda, S., and Shimizu, H., 2000, JNdi-1: a neodymium isotopic reference in consistency with LaJolla neodymium. Chemical Geology, 168, 279–281.

Tchameni, R., Sun, F., Dawaï, D., Danra, G., Tékoum, L., Nomo Negue, E., Vanderhaeghe, O., Nzolang, C., and Dagwaï Nguihdama, 2016, Zircon dating and mineralogy of the Mokong Pan-African magmatic epidote-bearing granite (North Cameroon). International Journal of Earth Sciences, 105, 1811–1830.

Tchuimegnie Ngongang, N.B., Kamgang, P., Chazot, G., Agranier, A., Bellon, H., and Nonnotte, P., 2015, Age, geochemical characteristics and petrogenesis of Cenozoic intraplate alkaline volcanic rocks in the Bafang region, West Cameroon. Journal of African Earth Sciences, 102, 218–232.

Thirlwall, M.F., 2000, Inter-laboratory and other errors in Pb isotope analyses investigated using a ^{207}Pb–^{204}Pb double spike. Chemical Geology, 163, 299–322.

Tiabou, A.F., Temdjim, R., Wandji, P., Bardintzeff, J.-M., Che, V.B., Tibang, E.E.B., Ngwa, N.C., and Mebara, O.F.X., 2019, Baossi-Warack monogenetic volcanoes, Adamawa Plateau, Cameroon: petrography, mineralogy and geochemistry. Acta Geochimica, 38, 40–67.

Tian, W., Campbell, I.H., Allen, C.M., Guan, P., Pan, W., Chen, M., Yu, H., and Zhu, W., 2010, The Tarim picrite-basalt-rhyolite suite, a Permian flood basalt from Northwest China with contrasting rhyolites produced by fractional crystallization and anatexis. Contributions to Mineralogy and Petrology, 160, 407–425.

Tsafack, J.-P.F., Wandji, P., Bardintzeff, J.-M., Bellon, H., and Guillou, H., 2009, The Mount Cameroon stratovolcano (Cameroon Volcanic Line, central Africa): petrology, geochemistry, isotope and age data. Geochemistry, Mineralogy and Petrology, 47, 65–78.

Wang, K., Plank, T., Walker, J.D., and Smith, E.I., 2002, A mantle melting profile across the basin and range, SW USA. Journal of Geophysical Research, 107, 1–21.

Weaver, B.L., 1991, The origin of ocean island basalt end-member compositions: trace element and isotopic constraints. Earth and Planetary Science Letters, 104, 381–397.

Wendt, J.I., Regelous, M., Niu, Y.L., Hekinian, R., and Collerson, K.D., 1999, Geochemistry of lavas from the Garrett Transform Fault: insights into mantle heterogeneity beneath the eastern Pacific. Earth and Planetary Science Letters, 173, 271–284.

Wigger, P.J., Schmitz, M., Araneda, M., Asch, G., Baldzuhn, S., Giese, P., Heinsohn, W.-D., Martinez, E., Ricaldi, E., Rower, P., and Vira-

monte, J., 1994, Variation in the crustal structure of the southern central Andes deduced from seismic refraction investigations. In: Reutter, K.-J., Scheuber, E., and Wigger, P.J. (eds.), Tectonics of The Southern Central Andes: Structure and Evolution of an Active Continental Margin. Springer, Berlin, p. 23–48, https://doi.org/10.1007/978-3-642-77353-2_2

Willbold, M. and Stracke, A., 2006, Trace element composition of mantle end-members: implications for recycling of oceanic and upper and lower continental crust. Geochemistry, Geophysics, Geosystems, 7, 1–30.

Willbold, M. and Stracke, A., 2010, Formation of enriched mantle components by recycling of upper and lower continental crust. Chemical Geology, 276, 188–197.

Workman, R.K. and Hart, S.R., 2005, Major and trace element composition of the depleted MORB mantle (DMM). Earth and Planetary Science Letters, 231, 53–72.

Xu, C., Huang, Z., Qi, L., Fu, P., Liu, C., Li, E., and Gung, T., 2007, Geochemistry of Cretaceous granites from Mianning in the Panix region, Sichuan Province, southwestern China: implications for their generation. Journal of Asian Earth Sciences, 29, 737–750.

Yokoyama, T., Aka, F.T., Kusakabe, M., and Nakamura, E., 2007, Plume-lithosphere interaction beneath Mt. Cameroon volcano, West Africa: constraints from ^{238}U-^{230}Th-^{226}Ra and Sr-Nd-Pb isotope systematics. Geochimica et Cosmochimica Acta, 71, 1835–1854.

Yokoyama, T., Makishima, A., and Nakamura, E., 1999, Separation of thorium and uranium from silicate rock samples using two commercial extraction chromatographic resins. Analytical Chemistry, 71, 135–141.

Yokoyama, T., Nagai, Y., Hinohara, Y., and Mori, T., 2017, Investigating the influence of nonspectral matrix effects for the determination of 22 trace elements in rock samples by ICP-QMS. Geostandards and Geoanalytical Research, 41, 221–242.

Zheng, J.P., Sun, M., Lu, F.X., and Pearson, N., 2003, Mesozoic lower crustal xenoliths and their significance in lithospheric evolution beneath the Sino-Korean craton. Tectonophysics, 361, 37–60.

Zindler, A. and Hart, S., 1986, Chemical geodynamics. Annual Review of Earth and Planetary Sciences, 14, 493–571.

Zou, H., Zindler, A., Xu, X., and Qi, Q., 2000, Major, trace element, and Nd, Sr and Pb isotope studies of Cenozoic basalts in SE China: mantle sources, regional variations, and tectonic significance. Chemical Geology, 171, 33–34.